

Lymphatic-derived oxysterols promote anti-tumor immunity and response to immunotherapy in melanoma

Received: 4 December 2023

Accepted: 7 January 2025

Published online: 31 January 2025

 Check for updates

Mengzhu Sun¹, Laure Garnier¹, Romane Chevalier¹, Martin Roumain², Chen Wang^{1,17}, Julien Angelillo¹, Julien Montorfani¹, Robert Pick¹, Dale Brighthouse¹, Nadine Fournier³, David Tarussio^{4,5,6}, Stéphanie Tissot^{4,5,6}, Jean-Marc Lobaccaro^{7,8,9}, Tatiana V. Petrova^{6,10}, Camilla Jandus^{1,6,11,12}, Daniel E. Speiser¹⁰, Manfred Kopf¹³, Caroline Pot¹⁴, Christoph Scheiermann^{1,11,12,15}, Krisztian Homicsko¹⁰, Giulio G. Muccioli², Abhishek D. Garg¹⁶ & Stéphanie Hugues^{1,11,12} ✉

In melanoma, lymphangiogenesis correlates with metastasis and poor prognosis and promotes immunosuppression. However, it also potentiates immunotherapy by supporting immune cell trafficking. We show in a lymphangiogenic murine melanoma that lymphatic endothelial cells (LECs) upregulate the enzyme Ch25h, which catalyzes the formation of 25-hydroxycholesterol (25-HC) from cholesterol and plays important roles in lipid metabolism, gene regulation, and immune activation. We identify a role for LECs as a source of extracellular 25-HC in tumors inhibiting PPAR- γ in intratumoral macrophages and monocytes, preventing their immunosuppressive function and instead promoting their conversion into proinflammatory myeloid cells that support effector T cell functions. In human melanoma, LECs also upregulate Ch25h, and its expression correlates with the lymphatic vessel signature, infiltration of pro-inflammatory macrophages, better patient survival, and better response to immunotherapy. We identify here in mechanistic detail an important LEC function that supports anti-tumor immunity, which can be therapeutically exploited in combination with immunotherapy.

Lymphangiogenesis is a hallmark of many solid tumors. The expansion of tumor lymphatic vessels (LVs) is largely mediated by VEGF-C and its receptors VEGFR-2/3, and high VEGF-C levels in the tumor microenvironment (TME) increase lymph node (LN) metastasis¹. In preclinical tumor models, an increase in VEGF-C signaling enhances metastatic dissemination to LNs and/or distal organs (reviewed in ref. 2). In addition, increased lymphatic drainage from the primary solid tumor to the sentinel LNs induces intra-LN LV expansion, associated with the formation of a “pre-metastatic niche” that favors metastatic cell colonization^{3,4}. LVs further impact anti-tumor immunity. First, LVs drain antigens and

antigen-presenting dendritic cells (DCs) to LNs and are, therefore, essential for the initiation of anti-tumor T-cell responses. However, tumor lymphatic endothelial cells (LECs) upregulate immunoregulatory molecules such as PD-L1 and MHCII to limit T cell-mediated immunity (especially against self-antigens), and hence their high density in tumors is associated with immunosuppression⁵⁻⁷. Finally, VEGF-C-induced lymphangiogenesis combined with immunotherapy approaches, including vaccination or PD-1 blockade, promote tumor-specific T cell immunity in tumor mouse models⁸⁻¹⁰. These results suggest that LECs are sensitive to the TME and that their high level of plasticity allows

A full list of affiliations appears at the end of the paper. ✉ e-mail: stephanie.hugues@unige.ch

them to adopt different phenotypes that can differentially impact tumor and immune cells.

Our RNA sequencing data indicates that, among other genes, LECs in murine melanoma upregulate the enzyme cholesterol 25-hydroxylase (Ch25h). *Ch25h* is an interferon-stimulated gene oxidizing cholesterol, and its primary product 25-hydroxycholesterol (25-HC) exhibits a broad-spectrum antiviral activity, by inducing membrane modifications blocking virus-cell interactions¹¹. Specifically, 25-HC inhibits the lipid-condensing effects of cholesterol, rendering the lipid bilayers less rigid. 25-HC further exhibits functions in modulating the inflammatory response. On one hand, it enhances the expression of IL-8, IL-6, CCL5, and CSF1, while on the other hand inhibits the production of IL-1 β due to an effect on sterol regulatory element-binding proteins (SREBP)¹². In vitro, 25-HC regulates transcriptional responses in macrophages and acts as an amplifier of inflammation via AP-1. In vivo, Ch25h^{KO} mice exhibit dampened inflammatory responses in influenza-infected mice¹³.

In the context of tumor development, oxysterols can exert both pro- and anti-tumorigenic functions in vitro¹⁴. In patients, low expression of Ch25h has been correlated with poor disease outcomes in colorectal cancer¹⁵. Studies have described that tumor-derived extracellular vesicles (TEVs) dampen the expression of Ch25h in the TME and educate healthy cells to function as premetastatic niches and to promote metastasis¹⁶. Furthermore, Ch25h expression in endothelial cells (ECs) dampens tumor-associated angiogenesis in melanoma and CRC mouse models¹⁵. In addition, Ch25h expression in tumor-infiltrating cytotoxic T lymphocytes (CTLs) prevents trogocytosis with cancer cells, and consequently inhibits CTL fratricide by other CTLs¹⁷. Finally, tumor-derived factors downregulate Ch25h in phagocytes, promoting phagolysosome fusion and dampening the cross-presentation of tumor antigens by the intratumoral DCs¹⁸. Altogether, these studies highlight a role for Ch25h expression and intracellular 25-HC in promoting CTL and DC functions, and inhibiting metastasis. However, whether and how the upregulation of Ch25h by LECs and the subsequent release of 25-HC in the TME will impact the tumor-associated lymphatic vasculature and anti-tumor immunity is unknown.

Here, we assess the impact of Ch25h expression by LECs in lymphangiogenic murine melanoma on tumor growth and anti-tumor immunity. In these settings, LECs represent a source of extracellular 25-HC in tumors, and the specific Ch25h abrogation in LECs induces a significant reduction of 25-HC levels. Subsequent 25-HC deprivation in the TME leads to a polarization of tumor-associated myeloid cells towards an immunosuppressive phenotype and prevents them from supporting effector T cells controlling tumor growth. Mechanistically, tumor LEC-derived 25-HC inhibits PPAR- γ in macrophages and monocytes and allows them to differentiate into proinflammatory iNOS⁺ myeloid cells in the TME. Importantly, the whole pathway, from the upregulation of Ch25h expression in tumor LECs to the promotion of immunogenic myeloid cells, enhanced T cell responses, and better control of tumor growth, is amplified upon immunotherapy, i.e., vaccination or adoptive T cell transfer. This suggests that protocols aiming at reinvigorating anti-tumor immunity can also promote LEC-immunogenic functions through the production of 25-HC. LECs in human melanoma express Ch25h, and levels of expression correlate with better response to ICB therapy. Our results highlight a role of extracellular oxysterols in strengthening and boosting anti-tumor immunity.

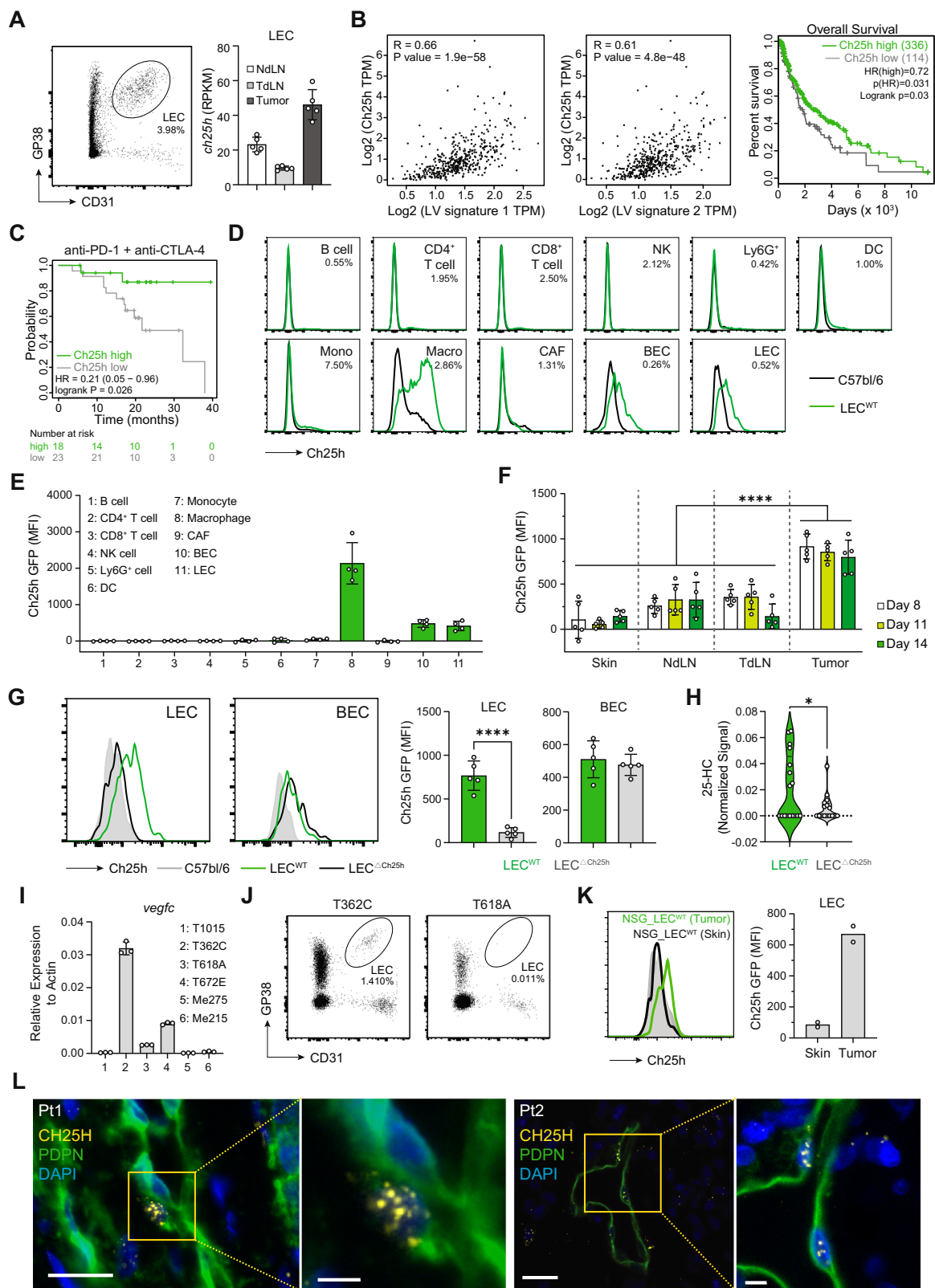
Results

Tumor LECs upregulate Ch25h and contribute to extracellular 25-hydroxycholesterol levels in lymphangiogenic melanoma

To assess LEC immunomodulatory functions in lymphangiogenic melanoma, we have used B16F10-OVA tumors overexpressing VEGF-C (B16F10-OVA VEGF-C), which, upon inoculation in mice, exhibit

increased density of tumoral LECs compared to parental B16F10-OVA tumors^{5,19}. Tumor cells were inoculated in C57BL/6 mice, and RNA sequencing was performed on LECs sorted from tumors, tumor-draining LNs (TdLN) and non-draining LNs (NdLN) on day 11. Principal component analysis showed that LECs in different organs exhibited a tissue-specific signature, which was further affected by the TME (Supplementary Fig. 1A). Over 3000 genes were dysregulated in tumor LECs compared to TdLN or NdLN (Supplementary Fig. 1A). Cholesterol 25-hydroxylase (Ch25h) mRNA was upregulated in tumor LECs compared to TdLN LECs and NdLN LECs (Fig. 1A). We have previously published that Ch25h expression in central nervous system (CNS) endothelial cells promotes neuroinflammation by inhibiting immunosuppressive myeloid cells²⁰. In addition, studies have shown that Ch25h expression in the TME impacts anti-tumor immunity^{15–18}. Importantly, TCGA datasets indicate that Ch25h mRNA expression in tumors positively correlates with LV signatures (LV signature 1: *pdpn*, *vegfc*, *lyve1*, and LV signature 2: *prox1*, *flt4*, *lyve1*, *pdpn*, *vegfc*) in melanoma patients (Fig. 1B). Overall survival (OS) was improved in melanoma patients with high tumoral Ch25h expression (top 25% cutoff) compared to relatively lower expression (bottom 75% cutoff) (Fig. 1B). Although standalone PD-1 or CTLA-4 blockade treatments did not have significant positive predictive activity related to Ch25h levels in melanoma patients (Supplementary Fig. 1B), Ch25h shows strong and significant effect in a large integrated dataset of melanoma patients that received PD-1 + CTLA-4 co-blockade^{21,22} (Fig. 1C). This indicates that Ch25h expression correlates with a better response to the immune checkpoint blockade (ICB)-based combinatorial regimen.

Flow cytometry on B16F10-OVA VEGF-C tumors inoculated in Ch25h-GFP^{loxP} fluorescent reporter mice (Supplementary Fig. 1C)²⁰, revealed that whereas different cells in the TME (Supplementary Fig. 1D) were mostly GFP negative (Fig. 1D, E), macrophages were the main expressors, followed by blood endothelial cells (BECs) and LECs, which expressed significant and comparable levels of Ch25h (Fig. 1D, E). In addition, tumor cells expressed negligible levels of Ch25h mRNA ex vivo (Supplementary Fig. 1E). Immunofluorescent staining on B16F10-OVA VEGF-C tumor sections further confirmed that LECs, BECs, and macrophages express Ch25h protein (Supplementary Fig. 1F). Analysis of LECs from skin, tumors, TdLNs, and NdLNs at different time points after tumor inoculation confirmed that Ch25h protein expression was significantly upregulated in tumor LECs compared to the other sites (Fig. 1F), and further showed that tumor LECs not only expressed high Ch25h levels already at day 8 after tumor inoculation, but further maintained elevated levels over the course of tumor growth (Fig. 1F). Of note, Ch25h expression levels in BECs followed a pattern that was comparable to LECs (Supplementary Fig. 1G). To determine the role of Ch25h expression by LECs in tumors, Ch25h-GFP^{loxP} mice were crossed with Prox1Cre^{ERT2} mice²³ (LEC Δ Ch25h mice). Ch25h-GFP^{loxP} mice were used as controls (LEC^{WT} mice). Upon tamoxifen treatment, Ch25h protein expression was efficiently abrogated in tumor LECs from LEC Δ Ch25h mice compared to LEC^{WT} mice (Fig. 1G), whereas its expression by tumor BECs was not affected (Fig. 1G). Flow cytometry analysis showed that LEC density was unaffected in LEC Δ Ch25h and LEC^{WT} tumors (Supplementary Fig. 2A), and Lyve-1 staining on LEC Δ Ch25h and LEC^{WT} tumor sections did not indicate any alterations of the LV structure after Ch25h abrogation in LECs (Supplementary Fig. 2B). In addition, draining of Alexa Fluor 488-dextran from tumor to tumor-draining LNs was unaffected in LEC Δ Ch25h mice compared to LEC^{WT} mice (Supplementary Fig. 2C). Therefore, abrogation of Ch25h in LECs does not affect gross LV vasculature and drainage function, suggesting that 25-HC has no major intracellular impact on LEC themselves. Accordingly, bulk RNA sequencing on LECs sorted from tumors in LEC Δ Ch25h and LEC^{WT} mice showed high sample similarity between the two groups (Supplementary Fig. 2D). Besides confirming an efficient deletion of Ch25h in LECs from LEC Δ Ch25h mice



(Supplementary Fig. 2E), data revealed very few differentially expressed genes (Supplementary Fig. 2F). None of these genes, except *vcam1*, are implicated in LV structure and functions. However, *vcam1* expression levels were negligible in all samples compared to highly expressed genes such as *ch25h*, *lyve1*, *prox1*, *icam1*, and *pecam1* (Supplementary Fig. 2G). These results are in agreement with the fact that *vcam1* is not expressed by LV capillaries and plays a

functional role in LV collectors²⁴, indicating that its differential expression between tumor LECs from LEC Δ Ch25h and LEC^{WT} mice has no major effect on tumor LV functions.

Altogether, these results show that Ch25h abrogation in LECs does not affect their structure and drainage functions in tumors. In contrast, lipid spectrometry analysis on tumor interstitial fluid showed that 25-HC levels were significantly reduced in LEC Δ Ch25h tumors compared to

Fig. 1 | LECs express Ch25h and control extracellular 25-hydroxycholesterol (25-HC) levels in lymphangiogenic B16F10-OVA tumors. **A** B16F10-OVA VEGF-C tumors were inoculated in C57BL/6 mice. LECs were sorted by flow cytometry (CD45^{neg}CD31^{GP38}) from tumors, tumor-draining LNs (TdLN) and non-draining LNs (NdLN) after 11 days. Ch25h mRNA levels (RPKM) provided by RNA sequencing, $n = 5$ mice/group. Data were presented as mean values \pm SD. **B** Correlation between Ch25h expression and lymphatic vessel (LV) signature (LV signature 1: *pdpn*, *vegfc*, *lyve1*, and LV signature 2: *prox1*, *flt4*, *lyve1*, *pdpn*, *vegfc*) in SKCM (Skin cutaneous melanoma) patients (TPM transcript per million). SKCM patient overall survival (OS) of high and low Ch25h expression. Data extracted from TCGA. **C** Predictive activity (OS) of Ch25h high and Ch25h low-expressors SKCM patients treated with anti-PD-1 and anti-CTLA-4, from an integrated dataset of multiple clinical trial studies. Significance was determined by log-rank analysis. **D–F** B16F10-OVA VEGF-C tumor cells were injected into Ch25h-GFP and WT mice. **D**, **E** Ch25h expression by tumor infiltrated cells on day 14. (DC dendritic cells, CAF cancer-associated fibroblasts, BEC blood endothelial cells). Results are representative of two independent experiments, with $n = 4$ mice/group. **F** Ch25h expression by LECs in indicated

organs at different time points. Results are pooled from two independent experiments, with $n = 2–3$ mice/group each. Two-way ANOVA, **** $P < 0.0001$. **G**, **H** B16F10-OVA VEGF-C tumor cells were injected in LEC^{ΔCh25h} and LEC^{WT} mice. **G** Ch25h expression by LECs and BECs in tumors on day 11. Results are representative of two independent experiments, with $n = 5$ mice/group. **D–G** Ch25h expression is represented as MFI Ch25h-GFP – MFI-WT mice. **H** 25-HC levels in tumor interstitial fluid measured by liquid chromatography–mass spectrometry. Results are pooled from two experiments, with $n = 4–13$ mice /group. **G**, **H** Two-tailed unpaired *t*-test. * $P < 0.05$; **** $P < 0.0001$. **I** VEGF-C expression in human melanoma cell lines by Q-PCR. Histograms depict technical triplicates from one experiment. **E–I** Data were presented as mean values \pm SD. **J**, **K** Human melanoma VEGF-C^{high} T362C and VEGF-C^{low} T618A cells were injected in NSG (WT), NSG-LEC^{ΔCh25h}, and NSG-LEC^{WT} mice. Ch25h expression (MFI Ch25h-GFP-MFI-WT mice) by LECs from tumors and skin was assessed by flow cytometry. Data were presented as mean values \pm SD. Results are representative of two independent experiments. **L** Ch25h mRNA and PDPN staining on human melanoma sections ($n = 3$ patients). Representative images are shown for patients 1 (Pt1) and 2 (Pt2). Scale bar, 20 and 5 μ m (zoomed).

LEC^{WT} tumors (Fig. 1H). This indicates that, although they are not the main Ch25h expression in the TME, LECs significantly contribute to extracellular 25-HC levels in B16F10-OVA VEGF-C tumors. Accordingly, primary cultured WT LECs exposed to B16F10-OVA VEGF-C tumor cell conditioned medium (TCM) potently released 25-HC in vitro compared to Ch25h knockout LECs (Supplementary Fig. 2H). This was not the case for WT BMDMs, which, similar to Ch25h knockout BMDMs, did not release detectable levels of 25-HC extracellularly when exposed to TCM (Supplementary Fig. 2H). In addition, 25-HC was detected in the culture supernatant of b.END3 mouse brain EC line exposed to TCM, suggesting that BECs can produce extracellular 25-HC (Supplementary Fig. 2H). These in vitro results suggest that 25-HC produced by LECs and BECs can be secreted, while macrophages likely maintain this metabolite intracellularly. Systemic levels of 25-HC in sera of B16-OVA VEGF-C tumor mice were not affected in LEC^{ΔCh25h} mice compared to controls (Supplementary Fig. 2I) and were lower compared to local tumor levels (Fig. 1H). These results demonstrate that LEC-specific depletion of Ch25h controls 25-HC in the TME without inducing variation of systemic 25-HC levels (which are relatively low). Ch25h is also implicated in the production of 7-keto-25-hydroxycholesterol (7-keto-25-HC)²⁵. 7-keto-25-HC was decreased in B16-OVA VEGF-C tumors from LEC^{ΔCh25h} compared to LEC^{WT} mice (Supplementary Fig. 2J), however, its levels in the TME remained abundant compared to 25-HC (Fig. 1H).

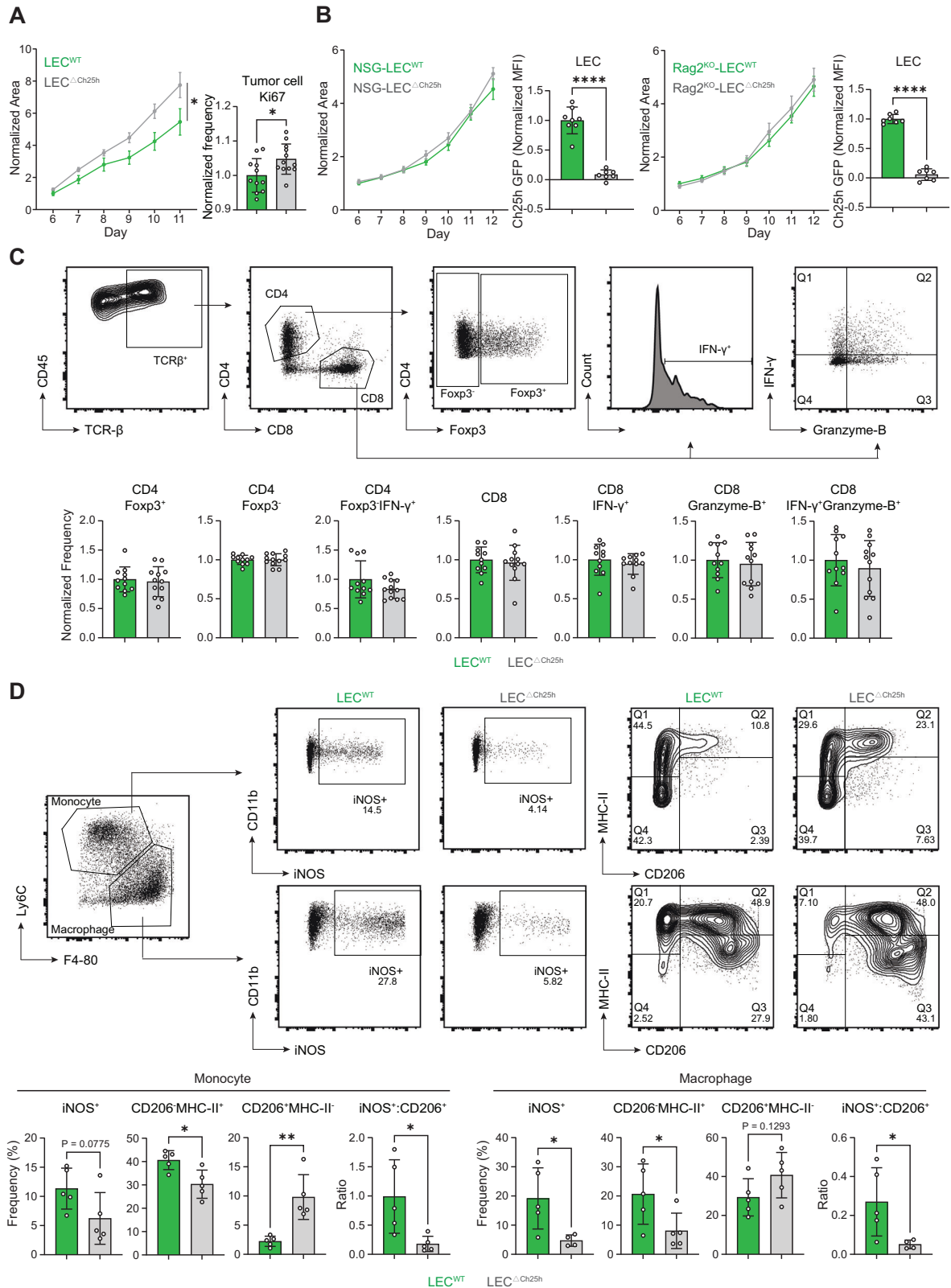
To determine whether our findings translate to human tumors, VEGF-C production was assessed by measuring VEGF-C mRNA levels in a panel of human melanoma cell lines (Fig. 1I). Some of the cell lines did not express detectable *vegfc* (T1015, Me275, Me215) or only low levels (T618A), while others (T362C, T672E) showed significant expression of *vegfc* (Fig. 1I). To assess if the in vitro measured VEGF-C mRNA expression were biologically relevant in promoting LV formation in an in vivo tumor setting, VEGF-C^{high} T362C and VEGF-C^{low} T618A human melanoma cells were implanted into immune-compromised NSG mice crossed with Ch25h-GFP^{loxP} fluorescent reporter (NSG-LEC^{WT}). In contrast to VEGF-C^{low} T618A cells, VEGF-C^{high} T362C human melanoma induced detectable amounts of tumoral LECs (Fig. 1J). Strikingly, LECs upregulated Ch25h in T362C lymphangiogenic tumors compared to skin LECs (Fig. 1K). These results show that melanoma patient-derived cell lines produce VEGF-C that supports LV sprouting in the TME of mice in vivo, and the upregulation of Ch25h in mouse LECs. Importantly, we also detected Ch25h mRNA in LECs from human melanoma (Fig. 1L).

Ch25h expression by tumor LECs controls tumor growth by impacting anti-tumor immunity

We next tested the impact of Ch25h abrogation in LECs on B16F10-OVA VEGF-C tumor development. Tumor growth was significantly increased, and tumor cell proliferation enhanced, in LEC^{ΔCh25h} mice

compared to LEC^{WT} mice (Fig. 2A). Increased tumor growth in LEC^{ΔCh25h} mice compared to LEC^{WT} mice was also observed in parental B16F10, and in models of colorectal adenocarcinoma (ectopic subcutaneous MC38 and MC38 VEGF-C^{high}, orthotopic intrarectal MC38) and breast cancer (orthotopic mammary fat pad E0771) (Supplementary Fig. 3A). These results demonstrate that Ch25h expression by LECs controls the growth of other tumors and is not restricted to OVA expressing or to VEGF-C overexpressing tumors (% of LEC among CD45^{neg} cells = 9.562 ± 5.963 ; % of LEC among live cells = 0.5275 ± 0.3225). In addition, Ch25h GFP⁺ expression was detected in tumor LECs in parental B16F10 (% of LEC among CD45^{neg} cells = 0.029 ± 0.053 ; % of LEC among live cells = 0.0043 ± 0.0049), orthotopic MC38 (LEC% among CD45^{neg} cells = 0.244 ± 0.140 ; % of LEC among live cells = 0.0166 ± 0.0084) and ectopic MC38 VEGF-C^{high} (% of LEC among CD45^{neg} cells = 0.475 ± 0.250 ; % of LEC among live cells = 0.0081 ± 0.0059) tumors (Supplementary Fig. 3B). In these tumor models, macrophages are more or less abundant (%: 2.252 ± 1.092 in B16F10, 10.823 ± 7.277 in MC38 and 0.980 ± 0.930 in MC38 VEGF-C^{high} tumors) and are the main expression of Ch25h (Supplementary Fig. 3B). In ectopic MC38 and orthotopic E0771 tumors, however, LEC numbers were too low to be detected by flow cytometry.

Differences in B16F10-OVA VEGF-C tumor growth were abrogated when LEC^{ΔCh25h} and LEC^{WT} mice were crossed on either NSG or Rag2^{KO} background (Fig. 2B). Ch25h was nevertheless expressed in tumoral LECs from NSG-LEC^{WT} and Rag2^{KO}-LEC^{WT} mice and abrogated in NSG-LEC^{ΔCh25h} and Rag2^{KO}-LEC^{ΔCh25h} mice (Fig. 2B). Therefore, the anti-tumorigenic effect of 25-HC is immune cell-dependent, although Ch25h expression can be induced in tumoral LECs in the absence of immune cells. Accordingly, B16F10-OVA VEGF-C tumor growth was not only increased in LEC^{ΔCh25h} mice (Fig. 2A and Supplementary Fig. 4A), but the CD45⁺/tumor cell ratio was significantly decreased in tumors from LEC^{ΔCh25h} compared to tumors from LEC^{WT} mice (Supplementary Fig. 4A). Therefore, our data indicates that Ch25h expression by LECs dampens B16F10-OVA VEGF-C tumor growth by impacting anti-tumor immunity. Furthermore, tumor growth difference being abrogated in a Rag2^{KO} background, this phenotype likely requires B and/or T cell-mediated immunity. B-cell depletion did not abolish B16F10-OVA VEGF-C tumor growth difference in LEC^{WT} and LEC^{ΔCh25h} mice (Supplementary Fig. 4B), suggesting that T-cell responses are essential. Ch25h-derived metabolite 25-HC can be further metabolized by the enzyme Cyp7b1 into 7 α -25-HC, which is a ligand for the G-protein coupled receptor Epstein-Barr virus-induced gene 2 (EBI2)²⁶ that induces chemotactic migration of a large variety of immune cells^{27–29}. A negligible level of Cyp7b1 mRNA was found in tumoral LECs by RNaseq or by Q-PCR (Supplementary Fig. 4C). In addition, B16F10-OVA VEGF-C tumors transplanted in mixed bone marrow (BM) chimeric mice (50% WT CD45.1⁺ BM cells + 50% EBI2^{KO}



CD45.1⁺/2⁺ BM cells) did not show any difference in the ratio of WT/EBI2^{KO} infiltrating immune cells compared to blood circulating cells (Supplementary Fig. 4D), ruling out a role for EBI2-mediated immune cell recruitment in tumors in the impact of LEC-derived 25-HC on anti-tumor immunity.

In-depth analysis of B16F10-OVA VEGF-C tumor-infiltrating T cells did not show any significant difference in frequencies of

effector T cell populations in tumors from LEC^{WT} and LEC^{ΔCh25h} mice, such as CD4⁺ T cells producing IFN-γ, Treg, and CD8⁺ T cells or CD8⁺ T cells producing IFN-γ and Granzyme-B (Fig. 2C). Whereas some OVA-specific effector CD8⁺ T cells are detectable in tumors, no difference was observed in frequencies between LEC^{WT} and LEC^{ΔCh25h} mice (Supplementary Fig. 4E). These results were surprising, since differences in tumor growth between LEC^{WT} and LEC^{ΔCh25h} mice were

Fig. 2 | Loss of Ch25h expression by tumor LECs enhances tumor growth by dampening anti-tumor immunity. **A–D** B16F10-OVA VEGF-C cells were injected in LEC Δ Ch25h and LEC^{WT} mice (**A, C, D**), in NSG-LEC Δ Ch25h and NSG-LEC^{WT} mice, or in Rag2^{KO}-LEC Δ Ch25h and Rag2^{KO}-LEC^{WT} mice (**B**). **A, B** Tumor growth was followed and normalized to the size of tumors in LEC^{WT}, NSG-LEC^{WT}, and Rag2^{KO}-LEC^{WT} mice, respectively, at day 6 for tumor growth, two-way ANOVA, $P < 0.05$. Data were presented as mean values \pm SEM. Tumor cell proliferation (Ki67⁺) was evaluated by flow cytometry on day 11. Data were presented as mean values \pm SD. Results are pooled from two independent experiments ($n = 4–8$ mice per group each) and normalized to WT (**A**), and Ch25h expression (MFI Ch25h-GFP – MFI-WT mice) was measured by flow cytometry at day 12 (**B**). **C, D** Tumors were harvested on day 11.

CD4⁺ and CD8⁺ T cells were analyzed for their expression of indicated markers. Representative flow cytometry dot plots and histograms provide the frequency of positive cells among T cell subsets. Data are presented as mean values \pm SD. Results are pooled from two independent experiments ($n = 4–8$ mice/ group each) and normalized to WT. **D** Myeloid cells (CD11b⁺CD68⁺) were separated into monocytes (Ly6C⁺F4/80⁺) and macrophages (Ly6C⁺F4/80⁺) and were analyzed for their expression of indicated markers. Representative flow cytometry dot plots provide the frequency of positive cells among indicated cells. Data were presented as mean values \pm SD. Results are representative of two independent experiments, $n = 5–7$ mice/group each. **A–D** For FACS analysis, two-tailed unpaired *t*-test. $P < 0.05$; $^{*}P < 0.01$; $^{***}P < 0.0001$.

abrogated in a Rag2^{KO} background (Fig. 2A, B). This indicates that T cells may be needed to support or amplify other immune cell functions.

CD68⁺CD11b⁺ myeloid cells, further separated based on Ly6C and F4/80 expression to discriminate between monocytes (Ly6C⁺F4/80⁺) and macrophages (Ly6C⁺F4/80⁺), showed striking phenotypic differences between in tumors from LEC Δ Ch25h and LEC^{WT} mice. Both cell subsets demonstrated a significant shift toward an immunosuppressive state (CD206⁺) in LEC Δ Ch25h mice compared to LEC^{WT} mice for which tumors contained more pro-inflammatory monocytes and macrophages (CD206⁺MHCII⁺, iNOS⁺) (Fig. 2D). Therefore, in the absence of Ch25h expression by tumoral LECs, the phenotype of tumor-infiltrating monocytes and macrophages is biased towards an immunosuppressive phenotype. Supporting the hypothesis of T cells promoting anti-tumor monocyte and macrophage functions in LEC^{WT} mice, tumors in Rag2^{KO} mice exhibited an almost complete absence of iNOS⁺ monocytes or macrophages compared to WT tumors (Supplementary Fig. 4F). Consistent with an absence of contribution for B cells to the phenotype, the frequencies of iNOS⁺ monocytes and macrophages in tumors were not affected by the deletion of B cells (Supplementary Fig. 4G). Other innate leukocyte populations infiltrating tumors from LEC^{WT} and LEC Δ Ch25h mice showed a slight reduction in NK frequency, but did not reveal any further major difference, including DC and NK effector populations (Supplementary Fig. 4H). In contrast, although the frequency of total neutrophils (Ly6G⁺) was not affected, we observed a decrease in iNOS⁺ ones (Supplementary Fig. 4H).

Impaired response to immunotherapy in mice lacking Ch25h expression in LECs

B16F10 melanoma is often classified as an immunologically cold tumor³⁰. Having in mind that the expression of Ch25h in human melanoma correlates with a better response to immunotherapy (Fig. 1C), we reasoned that by mitigating immunogenicity of B16F10-OVA VEGF-C tumors, we might observe a superior impact of Ch25h expression by LECs on anti-tumor immune responses. To this aim, B16F10-OVA VEGF-C tumor-bearing LEC Δ Ch25h and LEC^{WT} mice were vaccinated with OVA protein combined with CpG-B. First, we observed that upon vaccination, tumor LECs from LEC^{WT} mice upregulated even further Ch25h (Fig. 3A). Interestingly, the vaccination did not potentiate Ch25h expression in BECs (Fig. 3A). In addition, whereas both LEC Δ Ch25h and LEC^{WT} mice efficiently controlled tumor growth the first 2 weeks of vaccination compared to unvaccinated controls (Fig. 3B), tumors relapsed in LEC Δ Ch25h mice, whereas LEC^{WT} mice can maintain small tumor sizes for up to 24 days at least, afterwards they may relapse (Fig. 3B and Supplementary Fig. 5A) possibly due to immune cell exhaustion. Tumor cell analysis revealed that the CD45⁺/tumor cell ratio and CD45 frequency in the tumor were decreased, whereas tumor cell proliferation was increased in vaccinated LEC Δ Ch25h mice compared to controls (Fig. 3C). Apart from CD206⁺MHCII⁺ monocyte frequencies, alterations toward an immunosuppressive phenotype of tumor-infiltrating monocytes and macrophages in LEC Δ Ch25h mice were mostly recapitulated upon vaccination (Fig. 3D) as in unvaccinated

mice (Fig. 2D), with significantly less iNOS⁺ in both monocytes and macrophages, and less CD206⁺MHCII⁺ cells in macrophages compared to LEC^{WT} mice. Consequently, the ratios iNOS⁺/CD206⁺ monocytes and macrophages were impaired in tumors of vaccinated LEC Δ Ch25h mice, with a more drastic effect on monocytes compared to macrophages (Fig. 3D). Strikingly, whereas differences in T cells were absent without vaccination (Fig. 2C), tumor-infiltrating IFN- γ and TNF- α producing effector CD8⁺ T cell frequencies were impaired in LEC Δ Ch25h mice, whereas PD-1⁺Tim-3⁺ exhausted CD8⁺ T cells were increased (Fig. 3E). Granzyme-B expression by CD8⁺ T cells was however not affected by the abrogation of Ch25h in LECs (Fig. 3E). IFN- γ producing CD4⁺ T cell (Th1) frequencies were significantly impaired in tumors in vaccinated LEC Δ Ch25h mice (Fig. 3E), while Treg frequencies were not altered (Fig. 3E). Although RNA sequencing data did not show any difference in the expression of genes related to antigen presentation between tumor LECs from LEC^{WT} and LEC Δ Ch25h mice (Supplementary Fig. 2F), it is possible that upon vaccination, LEC antigen-presentation functions were affected by the loss of Ch25h and contributed to the impact observed in T cell responses in tumors from LEC Δ Ch25h mice. LECs are well known to express negligible levels of co-stimulatory molecules³¹. We nevertheless assessed the frequency of MHCII positive cells, the expression levels of SIINFEKL-MHC-I complexes and PD-L1 in tumor LECs from LEC^{WT} and LEC Δ Ch25h mice (Supplementary Fig. 5B) and could not observe any difference. These results suggest that Ch25h expression by LECs does not modulate their ability to present antigens and does not contribute to differences in T cell responses in tumors from LEC^{WT} and LEC Δ Ch25h mice.

NK frequencies and effector functions (production of IFN- γ and Granzyme-B) appeared unaffected in tumors from vaccinated LEC Δ Ch25h mice compared to their controls (Supplementary Fig. 5C). DC and neutrophil (Ly6G⁺) frequencies were respectively increased and decreased in tumors from LEC Δ Ch25h mice, with however no difference in iNOS⁺ neutrophils (Ly6G⁺iNOS⁺) (Supplementary Fig. 5C), suggesting that some populations in the TME were affected by the loss of inflammatory myeloid cells and effector T cells in vaccinated LEC Δ Ch25h mice. In TdLNs, we could not find any difference in DC frequencies, SIINFEKL-MHC-I complexes expression levels by DCs, or effector T cell frequencies, and the frequencies of monocytes and macrophages expressing iNOS and CD206 were negligible (Supplementary Fig. 5D). Together with the fact that LECs express negligible levels of Ch25h in TdLNs, these data support a local modulation of tumor-infiltrating immune cells by Ch25h expressing LECs. Finally, LN metastasis was augmented in LEC Δ Ch25h mice (Supplementary Fig. 5E), probably due to primary tumor relapse, and not because of an alteration of the lymphatic vasculature associated with the tumor, which appears comparable in tumors from vaccinated LEC Δ Ch25h and LEC^{WT} mice (Supplementary Fig. 5F).

We tested a second approach of immunotherapy, the adoptive transfer of tumor-specific effector CD8⁺ T cells. In this setting, the priming phase of anti-tumor CD8⁺ T cells is bypassed, allowing a focus on the impact of Ch25h expression by LECs on effector T cells in tumors. Preactivated OT-1 cells injected intravenously into B16F10-OVA VEGF-C tumor-bearing mice were significantly

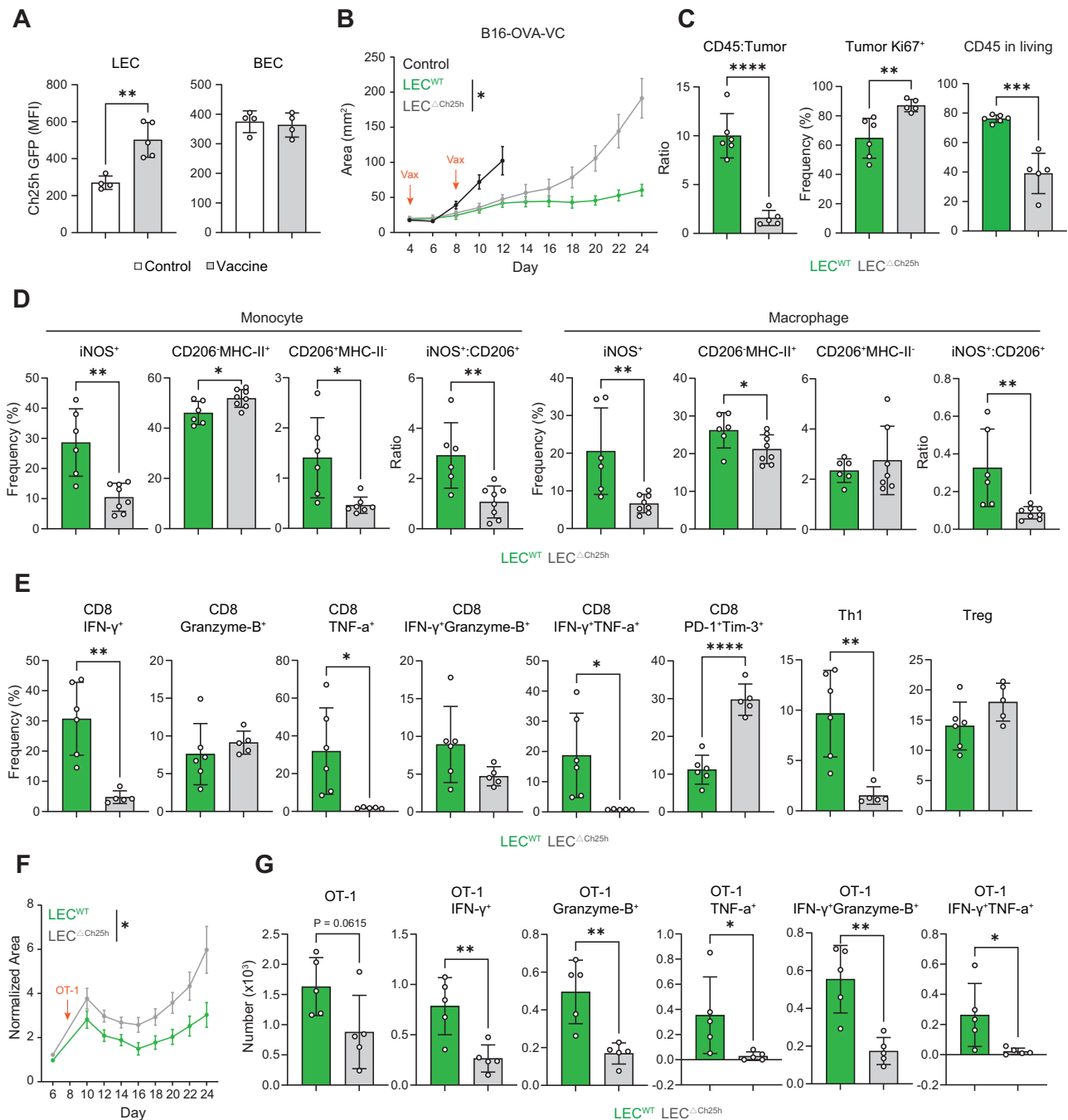
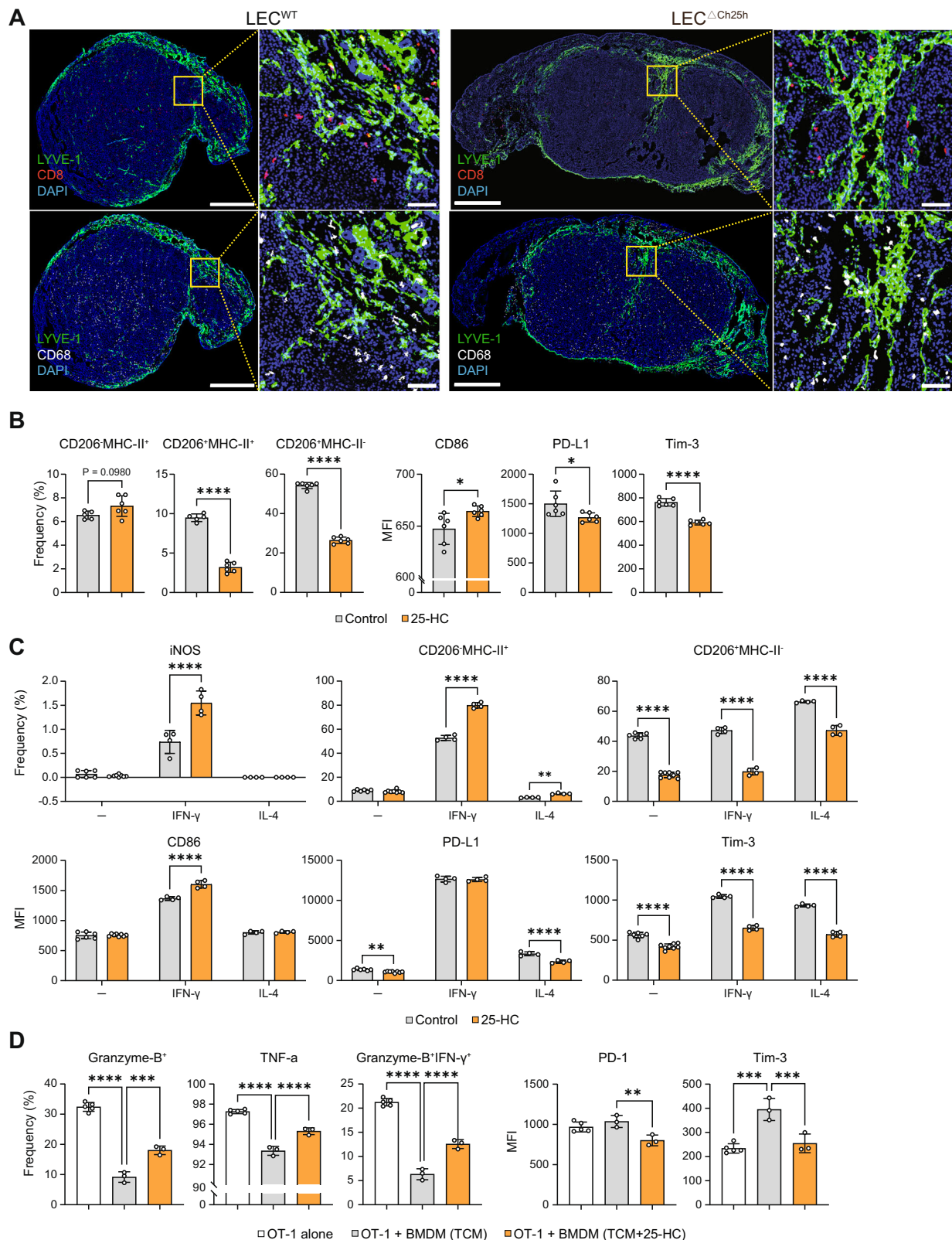


Fig. 3 | Loss of Ch25h in LECs dampens immunotherapy efficacy in lymphangiogenic melanoma. A–E LEC^{ΔCh25h} and LEC^{WT} mice were inoculated with B16F10-OVA VEGF-C (B16-OVA-VC) cells and vaccinated with OVA protein and CpG-B at day 5 (**A**) or at day 4 and day 8 (**B–E**). **A** Ch25h expression (GFP MFI) was measured by flow cytometry on day 11. $n = 5$ mice/group. **B** Tumor growth was followed and compared to unvaccinated B16F10-OVA VEGF-C tumor-bearing WT mice. Representative of four independent experiments, $n = 5–6$ mice/group each. **C–E** Tumor were harvested on day 24 and analyzed by flow cytometry. **C** CD45⁺/tumor cell ratio and tumor cell proliferation (Ki67⁺) and CD45⁺ cell frequency in living cells. **D** Myeloid cells (CD11b⁺CD68⁺) were separated into monocytes (Ly6C⁺F4/80⁻) and macrophages (Ly6C⁺F4/80⁺) and were analyzed for their

expression of indicated markers. **E** CD4⁺ and CD8⁺ T cells were analyzed for their expression of indicated markers. **C–E** Representative of two independent experiments, $n = 5–8$ mice/group each. Data were presented as mean values \pm SD (**F**, **G**) LEC^{ΔCh25h} and LEC^{WT} mice were inoculated with B16F10-OVA VEGF-C cells and adoptively transferred 8 days later with OT-1 effector T cells. Tumor growth was followed and normalized to the size of WT at day 6 (**F**), and OT-1 cells were analyzed in tumors 2 days after transfer for indicated markers (**G**). Data were pooled from two independent experiments, $n = 2–5$ mice/group each, and are presented as mean values \pm SEM (**F**) or as mean values \pm SEM (**G**). **B, F** Two-way ANOVA, $P < 0.05$. (**A, C, D, E, G**) Two-tailed unpaired t -test. * $P < 0.05$; ** $P < 0.01$; **** $P < 0.0001$.

less efficient at controlling tumor growth in LEC^{ΔCh25h} mice compared to LEC^{WT} controls (Fig. 3F). Already 2 days post-adoptive transfer, OT-1 cells infiltrating tumors exhibited reduced effector functions (lower numbers of IFN-γ⁺, TNF-α⁺, Granzyme-B⁺ cells) (Fig. 3G).

Altogether, our data suggest that upon vaccination or effector T cell transfer, the expression of Ch25h in tumor LECs induces the release of extracellular 25-HC in the TME and promotes anti-tumor activity of monocytes, macrophages, and effector T cells, resulting in a better response to immunotherapy.



25-HC alters the phenotype of tumor-associated myeloid cells *in vitro*

We next determined whether the expression of Ch25h by LECs in the TME has a direct effect on myeloid cells and/or T cells. Immunostaining on B16F10-OVA VEGF-C tumor sections revealed that both T cells and macrophages are positioned in proximity of LVs (Fig. 4A). Ch25h is responsible for the production of 25-HC and 7-keto-25-HC. Given that

extracellular 25-HC has been shown to impact macrophage phenotype *in vitro*³², whereas only an endogenous expression has been reported to alter T cell effectors¹⁷, we first tested *in vitro* the impact of 25-HC on tumor-conditioned BM-derived macrophages (BMDM). Flow cytometry experiments revealed that BMDM cultures exposed to tumor-conditioned medium (TCM) mostly exhibited an M2-like phenotype, with more than 70% expressing CD206 (MHCII⁺ or MHCII⁻) and

Fig. 4 | 25-HC treatment reverses tumor-associated macrophage immunosuppressive phenotype and functions in vitro. **A** LEC^{ΔCh25h} and LEC^{WT} mice were inoculated with B16F10-OVA VEGF-C cells and tumors were harvested at day 11. Montages of maximum projected 3D confocal images of representative sections ($n = 3$ mice/group) immunostained for lymphatic vessels (Lyve-1, green), T cells (CD8, red), myeloid cells (CD68, white), and nuclei (blue). Images were obtained using a 10x objective, including a 3x relative magnification. Selected regions of interest are indicated by dashed squares and denoted magnified areas are shown in images beside. Scale bars, 1 mm, 100 μ m (zoomed). **B** BMDMs were incubated with B16F10-OVA VEGF-C tumor-conditioned medium (TCM) and treated or not with 25-HC for 48 h. BMDM phenotype was analyzed by flow cytometry. Data were

representative of three independent experiments with $n = 3-6$ replicates each. Data were presented as mean values \pm SD. **C** BMDM were treated or not with IFN- γ or IL-4 and further treated or not with 25-HC for 48 h. BMDM phenotype was analyzed by flow cytometry. Data were representative of two independent experiments with $n = 4-8$ replicates each. Data were presented as mean values \pm SD. **D** TCM-exposed BMDM were treated or not with 25-HC for 48 h, washed, and incubated with OT-1 effector cells (5:1 ratio) for 48 h. T-cell phenotype was analyzed by flow cytometry. Data were representative of two independent experiments with $n = 3-5$ replicates each. Data were presented as mean values \pm SD. **E** Two-tailed unpaired *t*-test. **C** Two-way ANOVA, **D** One-way ANOVA. * $P < 0.05$; ** $P < 0.01$; *** $P < 0.001$; **** $P < 0.0001$.

contained very few MHCII⁺CD206⁻ cells (Fig. 4B), among which iNOS⁺ cells were undetectable in absence of further treatment (Fig. 4C). This is in line with the results obtained in Rag2^{KO} mice (Supplementary Fig. 4F), and probably due to the absence of inflammatory factors. 25-HC treatment significantly reduced the frequencies of CD206⁺ TCM-exposed BMDM, increased their CD86 expression, and further decreased their expression levels of Tim-3 and PD-L1 (Fig. 4B), molecules that have been shown to participate in immunosuppression mediated by macrophages^{33,34}. A modulation of TCM-exposed macrophages by 25-HC toward a less immunosuppressive phenotype as also confirmed by Q-PCR, with increased *cd86*, *cd80*, *il1b*, *tnf*, *il6*, *il12* mRNA expression levels, and decreased *myc*, *il10*, *tgfb1*, *mrc1*, *cd274*, and *havcr2* mRNA levels (Supplementary Fig. 6A). Although it has been shown that intracellular 25-HC acts as an antagonist of SREBP in macrophages, resulting in decreased IL-1 β production, our data suggest that extracellular 25-HC acts through a different mechanism and promotes IL-1 β production. In agreement, similar results (upregulation of *cd80*, *cd86*, *il1b*, *tnf*, *il6* and *il12* expression, downregulation of *mrc1*, *il10*, and *tgfb1*) were observed when TCM-exposed Ch25h^{-/-} BMDM were treated with 25-HC (Supplementary Fig. 6B).

The proportion of BMDM treated with the M1-polarizing cytokine IFN- γ that differentiated into iNOS⁺ cells, although represented at low frequency, was potentialized by the addition of 25-HC (Fig. 4C). Low iNOS⁺ cell frequencies might be explained by a lack of pro-inflammatory factors that need to synergize with IFN- γ and 25-HC to promote its expression. Frequencies of MHCII⁺CD206⁻ cells and the expression levels of CD86 (Fig. 4C), all hallmarks of pro-inflammatory, or immunogenic, macrophages were also enhanced. 25-HC did reduce Tim-3 expression by M1-polarized BMDM, without modulating PD-L1 levels, which directly respond to IFN- γ and were very high (Fig. 4C). In contrast to IFN- γ , pre-treatment of the M2-polarizing cytokine IL-4 increased the frequencies of CD206⁺ cells (Fig. 4C). The addition of 25-HC inhibited the polarization of immunosuppressive macrophages mediated by IL-4, with decreased CD206⁺, decreased PD-L1, and decreased Tim-3 (Fig. 4C). As previously shown³⁵, IFN- γ treatment induced upregulation of *ch25h* in BMDM (Supplementary Fig. 6C). However, Ch25h^{-/-} BMDM exhibited similar phenotypic modulation compared to WT BMDM (Fig. 4C) when exposed to polarizing cytokines IFN- γ or IL-4 and treated with 25-HC (Supplementary Fig. 6D), demonstrating that endogenous Ch25h expression does not contribute to the modulation of BMDM polarization induced by extracellular 25-HC. To determine whether alterations of phenotypes translate into impaired functions of macrophages, we further assessed their ability to modulate T cell effector and exhausted phenotypes. As published³⁶, tumor-conditioned BMDM significantly inhibited T cell effector functions (decreased frequencies of Granzyme-B⁺ and IFN- γ ⁺ OT-1 cells) and promoted a T cell exhausted phenotype (increased expression levels of Tim-3 and PD-1 by OT-1) (Fig. 4D). Strikingly, 25-HC pre-treatment of TCM-exposed BMDM significantly dampened their ability to inhibit effector T cells (Fig. 4D), which exhibited restored production of effector factors, and decreased expression of exhaustion markers, suggesting that in vivo, 25-HC might dampen the immunosuppressive functions of tumor-associated macrophages.

Although it remained elevated compared to 25-HC levels, 7-keto-25-HC was also reduced in the TME of LEC^{ΔCh25h} mice (Supplementary Fig. 2J). Therefore, we tested whether it could impact macrophage phenotype and functions. 7-keto-25-HC treatment induced minor modulations of BMDM phenotype (Supplementary Fig. 6E), however, it did not affect their ability to suppress effector T cells (Supplementary Fig. 6F). Altogether, these data suggest that 25-HC produced by LECs in the TME is a main regulator of tumor-associated myeloid cells.

LEC-derived 25-HC controls tumor growth by regulating myeloid cell functions

To determine whether myeloid cells are the primary cellular targets of LEC-derived 25-HC in vivo in tumors, and subsequently impact anti-tumor T cell responses, we depleted myeloid cells by injecting anti-CSF1R (CD115) antibodies³⁷ into B16F10-OVA VEGF-C tumor-bearing LEC^{ΔCh25h} and LEC^{WT} mice vaccinated as before. This treatment resulted in the depletion of 73% of macrophages and 25% of monocytes in LEC^{WT} tumors and 65% of macrophages and 51% of monocytes in LEC^{ΔCh25h} tumors (Supplementary Fig. 7A) and was sufficient to abrogate the difference in tumor size between LEC^{ΔCh25h} and LEC^{WT} mice (Fig. 5A). Upon myeloid cell depletion, vaccinated LEC^{WT} mice could not control the growth of tumors as efficiently (Fig. 5A). This suggests that in vaccinated LEC^{WT} mice, the net-effect of antibody-mediated cell depletion in tumors resulted in the elimination of anti-tumoral pro-inflammatory monocytes and macrophages. The TME of LEC^{WT} unvaccinated mice contains a balanced mix of pro- and anti-tumoral myeloid cells (Fig. 2D). As such, anti-CSF1R (CD115) antibody treatment in unvaccinated WT mice did not impact tumor growth (Supplementary Fig. 7B), suggesting that the net-effect of myeloid cell depletion was zero, with the depletion of both immunogenic and immunosuppressive myeloid cells. Next, we have used a reductionist approach to assess directly if the impact of LEC-derived 25-HC on tumor myeloid cells is indeed responsible for controlling tumor growth, by excluding the contribution from other immune cells in the TME. Immunodeficient (NSG) mice in which LECs express (NSG-LEC^{WT}) or not (NSG-LEC^{ΔCh25h}) Ch25h were transplanted with B16F10-OVA VEGF-C tumor cells mixed with BMDM or not. Tumor-bearing mice were next adoptively transferred with OT-1 effectors. NSG-LEC^{WT} and NSG-LEC^{ΔCh25h} mice transplanted with tumor cells alone and transferred with T cells exhibited an efficient and similar tumor growth regression, confirming that 25-HC released by LECs in the TME does not directly impact the ability of effector T cells to control tumor growth (Fig. 5B). In contrast, when co-transplanted with tumor cells and BMDM, compared to NSG-LEC^{WT} mice, NSG-LEC^{ΔCh25h} mice developed larger tumors (Fig. 5B).

These results, combined with our in vitro data (Fig. 4), demonstrate that myeloid cells represent the targets of 25-HC produced by LECs in the TME, resulting in a dampening of their immunosuppressive functions.

25-HC produced by LECs prevents the acquisition of an immunosuppressive phenotype by tumor-associated myeloid cells

Transcriptomic analysis of monocytes (CD11b⁺Ly6C⁺F4/80^{neg}) and macrophages (CD11b⁺Ly6C^{neg}F4/80⁺) sorted from B16F10-OVA VEGF-C

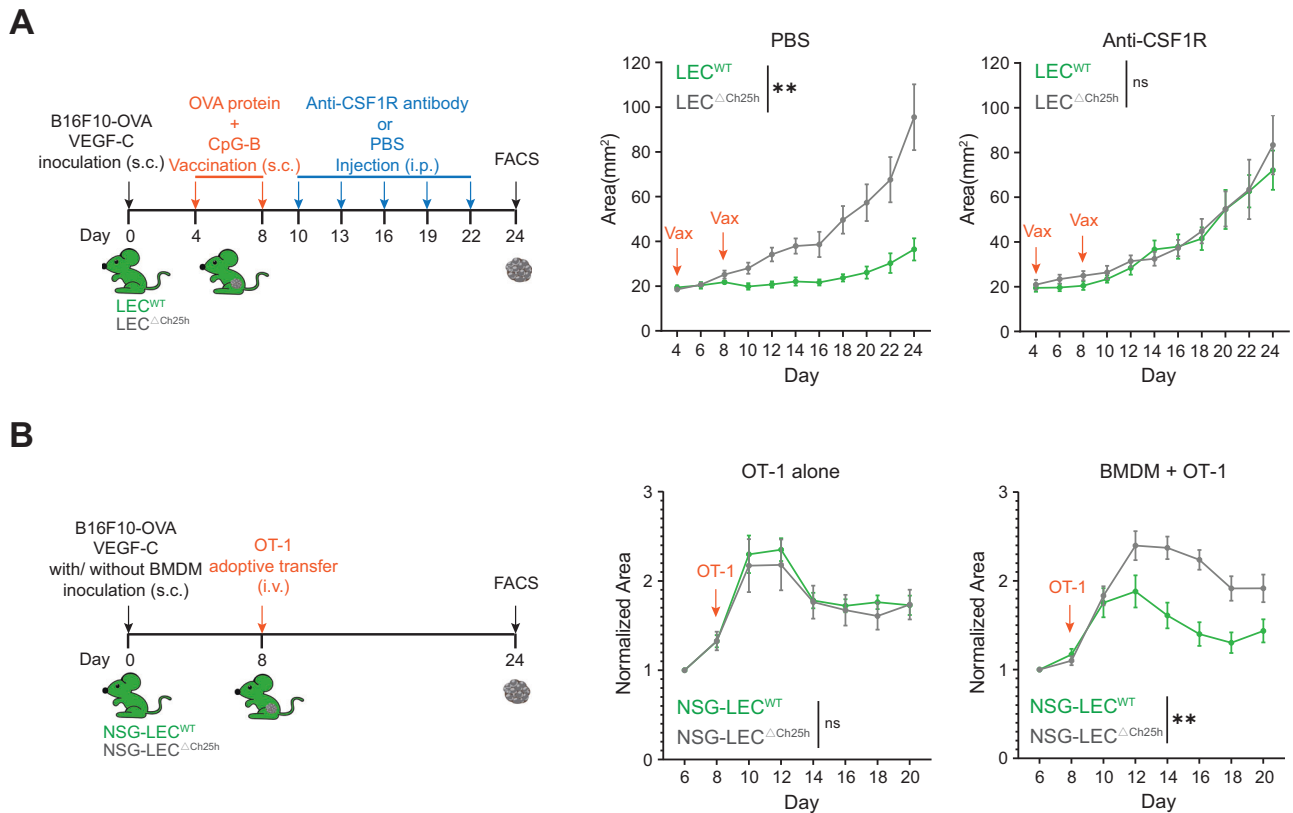
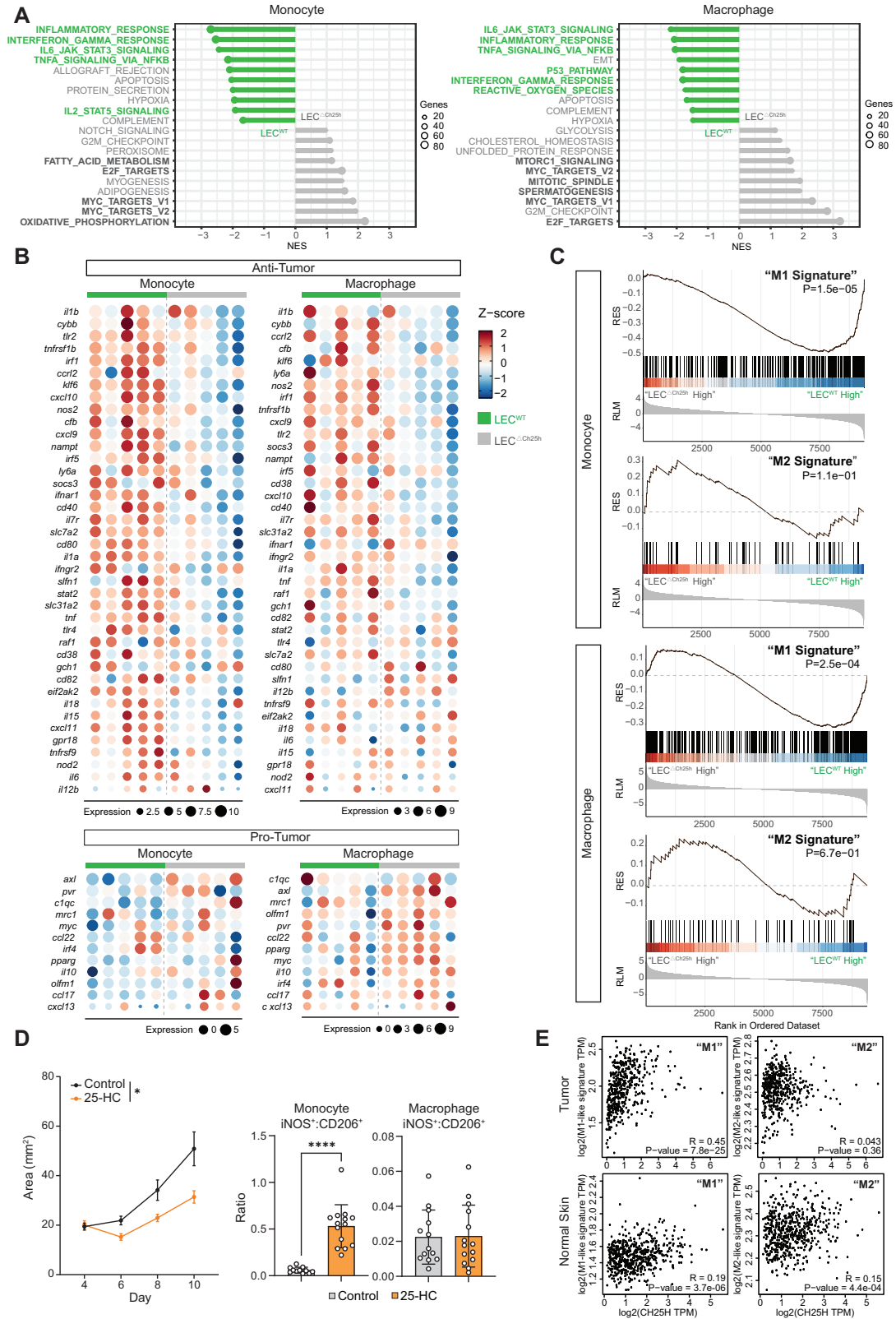


Fig. 5 | LEC-derived 25-HC modulates tumor growth by impacting tumor-associated macrophages and monocytes. A LEC^{ΔCh25h} and LEC^{WT} mice were inoculated with B16F10-OVA VEGF-C cells and vaccinated with OVA protein and CpG-B at day 4 and day 8. Mice were additionally injected with anti-CSF1R (1 mg / mouse) at day 10, followed by 500 μg/mouse every 3 days or PBS), as represented in the scheme. Tumor growth was followed. Two-way ANOVA, ***P* < 0.01. Data were representative of two independent experiments with *n* = 5–7 mice/group each.

B NSG-LEC^{ΔCh25h} and NSG-LEC^{WT} mice were inoculated with B16F10-OVA VEGF-C cells mixed or not with BMDM. Tumor-bearing mice were further adoptively transferred with OT-1 effectors on day 8, as represented in the scheme. Tumor growth was followed and normalized to the size individually from day 6. Two-way ANOVA, ***P* < 0.01. Data were pooled from two independent experiments with *n* = 5–8 mice/group each. **A, B** Data were presented as mean values ± SEM.

tumors after OVA+CpG-B vaccination revealed that their phenotype was strongly altered by the absence of Ch25h expression in LECs. First, most of the top ten Hallmark pathways expressed by monocytes in LEC^{WT} tumors were related to inflammation, such as inflammatory responses, IFN-γ response, IL-6/Jak/STAT3 signaling, TNF-α signaling via NF-KB and IL-2/STAT5 signaling (Fig. 6A). Similarly in tumor-infiltrating macrophages from LEC^{WT} mice, the top ten Hallmark pathways were related to inflammation and M1-like TAM signature, such as IL-6/Jak/STAT3 signaling, inflammatory response, TNF-α signaling via NF-KB, IFN-γ response, ROS pathway, P53 pathway³⁸ (Fig. 6A). In contrast, the 10 top pathways expressed by LEC^{ΔCh25h} tumor macrophages contained E2F targets that promote tumor cell metastasis³⁹, Myc-targets that mediate early glycolysis and dampen proinflammatory responses in macrophages by inhibiting IRF4⁴⁰, mTORC1 signaling that regulates proinflammatory macrophage function and metabolism^{41,42}, mitotic spindles, which seem to be a mutually exclusive events of NLRP3 activation⁴³, and spermatogenesis, a pathway containing known TAM receptors, such as Tyro3, Axl and MerTK, promoting M2 polarization and efferocytosis, two pro-tumoral processes^{44–47} (Fig. 6A). Interestingly, whereas in macrophages pathways related to metabolism were particularly expressed in LEC^{ΔCh25h} tumors (normalized enrichment score of 1.3 and 1.3 for cholesterol homeostasis and glycolysis, respectively), oxidative phosphorylation was the highest pathway upregulated in monocytes in LEC^{ΔCh25h} tumors (Fig. 6A). The fatty acid oxidation pathway was also upregulated in monocytes from LEC^{ΔCh25h} tumors (Fig. 6A). Knowing that M2-like myeloid cells undergo a metabolic reprogramming toward oxidative metabolism for bioenergetic purposes (OXPHOS)^{42,48}, and that

mitochondrial fatty acid oxidation has been associated with an immunosuppressive myeloid cell phenotype⁴⁹, it is tempting to speculate that the modulation of the “M2-like” phenotype by LEC-derived 25-HC might reprogram pro-resolving and pro-tumoral cells into more inflammatory anti-tumoral myeloid cells. Accordingly, by looking more precisely at the heatmaps generated with genes classified as “anti-tumor”, monocytes and macrophages present in tumors isolated from LEC^{WT} mice expressed a far more anti-tumor immune signature compared to LEC^{ΔCh25h} mice (Fig. 6B), with higher gene expression such as *Il1b*, *cxcl9*, *cxcl10*, *nos2*, and others. Other pro-inflammatory genes were also more expressed in monocytes and macrophages in LEC^{WT} compared to LEC^{ΔCh25h} tumors, such as, for example, *nlrp3* or (Supplementary Fig. 8A), although their role in tumor context remains unclear. In contrast, monocytes and macrophages in tumors from LEC^{ΔCh25h} mice upregulated genes clearly related to pro-tumoral immune functions, such as *Axl*, *Il10*, and *pparg* (Fig. 6B), with a more pronounced effect in macrophages compared to monocytes. Finally, monocytes and macrophages in LEC^{WT} tumors exhibited enrichment in genes described as “M1” signature by Pan W. et al., whereas monocytes and macrophages in LEC^{ΔCh25h} tumors showed an association with the “M2” signature⁵⁰ (Fig. 6C). No clear difference was observed in genes implicated in other myeloid cell functions, such as phagocytosis, or SERBP targets, between monocytes and macrophages isolated from LEC^{WT} and LEC^{ΔCh25h} tumors (Supplementary Fig. 8B). In order to determine whether 25-HC could be considered as a therapy to redirect the myeloid cells in vivo, we treated B16F10-OVA VEGF-C tumor-bearing mice intratumorally with 25-HC. We observed a better control of tumor growth in treated



animals compared to untreated controls (Fig. 6D). In addition, a shift toward more pro-inflammatory tumor-infiltrating myeloid cells was observed, as indicated by an increased ratio of iNOS⁺/CD206⁺ monocytes (Fig. 6D). We did not observe a significant change in macrophages, for which the ratio was very low.

Supporting a role for 25-HC in promoting anti-tumor macrophages in melanoma patients, we found that Ch25h showed a

significant positive correlation with an M1-like macrophage signature but no clear correlation with M2-like macrophage signature in the skin cutaneous melanoma (SKCM) TCGA dataset (Fig. 6E). In addition, although correlation of Ch25h with M2-signature was weak in both normal skin and tumor melanoma (R=0.15 and R=0.043, respectively), the correlation of Ch25h with M1-signature was much stronger in melanoma (R=0.45) compared to normal skin (R=0.19) (Fig. 6E),

Fig. 6 | Altered monocyte and macrophage transcriptomes in the absence of Ch25h expression by LECs in lymphangiogenic melanoma. **A–C** LEC^{ΔCh25h} and LEC^{WT} mice were inoculated with B16F10-OVA VEGF-C cells and vaccinated with OVA protein and CpG-B on day 4 and day 8. Tumors were harvested on day 24, and monocytes and macrophages were sorted by flow cytometry (see Fig. 2D for gating strategy). RNA sequencing was performed (Illumina). **A** Top 10 Hallmark pathways expressed in monocytes and macrophages in tumors from LEC^{ΔCh25h} and LEC^{WT} mice. **B** Heatmap showing expression levels of genes implicated in “anti-tumor” or “pro-tumor” immune signatures in monocytes and macrophages and in tumors from LEC^{ΔCh25h} and LEC^{WT} mice. **C** GSEA enrichment of M1 and M2 signatures in

monocytes and macrophages from tumor in LEC^{ΔCh25h} and LEC^{WT} mice using gene set from ref. 50. **D** B16F10-OVA VEGF-C tumor-bearing C57BL/6 mice were treated with 25-HC every 2 days, starting at day 4. Tumor growth was followed. Two-way ANOVA, **P* < 0.05. Data were a pool of three independent experiments with *n* = 4–6 mice/group each. On day 11, tumors were harvested, and the CD68⁺CD11b⁺ myeloid cell (macrophage, F4/80⁺Ly6C⁻ and monocytes, F4/80⁺Ly6C⁺) phenotype was assessed by flow cytometry. Ratio iNOS⁺/CD206⁺ cells are provided. Two-tailed unpaired *t*-test, ****p* < 0.001. **E** Correlation between Ch25h expression and M1/M2 signatures in normal skin and in SKCM patients. Data were extracted from the TCGA database.

indicating that Ch25h is not generally associated with M1 macrophages but rather only in tumoral or tumor-associated context.

LEC-derived 25-HC decreases PPAR-γ levels in tumor-associated macrophages to dampen their immunosuppressive functions

25-HC has been shown to mediate both LXR-dependent and -independent effects⁵¹. Therefore, we investigated whether this pathway is implicated in the ability of extracellular 25-HC to modulate macrophage phenotype and functions. In vitro, LXR deficient and WT BMDM pre-exposed to TCM and treated with 25-HC exhibited similar regulation of their phenotype, with decreased CD206⁺MHCII⁺ frequencies and decreased Tim-3 expression levels (Supplementary Fig. 9A) indicating that the impact of 25-HC on macrophages in tumoral context is LXR independent. In vivo, when co-inoculated with B16F10-OVA VEGF-C tumor cells into NSG mice, LXR deficient BMDM supported the control of tumor growth mediated by the transfer of OT-1 effectors as efficiently as WT BMDM (Supplementary Fig. 9B), confirming that 25-HC present in the TME promotes the ability of macrophages to control tumor growth independently of LXR.

Macrophages strongly upregulated PPAR-γ in B16F10-OVA VEGF-C tumors from LEC^{ΔCh25h} mice (Fig. 6B), which is well-known to exert an anti-inflammatory effect on macrophages by inhibiting AP-1/ NF-κB/ STAT1 pathways, COX-2, MPO, Caspase 3, and ROS production, and in contrast promoting OXPHOS and the production of anti-inflammatory cytokines^{42,52}. All these pathways being also modulated in myeloid cells infiltrating tumors from LEC^{ΔCh25h} and LEC^{WT} mice (Fig. 6A, B), and 25-HC having been shown to decrease PPAR-γ levels in vitro in THP-1 macrophages⁵³, we wondered whether this pathway could be implicated in the ability of 25-HC to prevent macrophage immunosuppressive phenotype and function. Accordingly, TCM-exposed BMDM treated with 25-HC downregulated PPAR-γ mRNA (Fig. 7A). As shown before, the addition of 25-HC inhibited the “M2-like” phenotype of TCM-exposed BMDM, inducing downregulation of CD206 (MHCII⁺ or MHCII⁺) and Tim-3 (Fig. 4B). Supporting the hypothesis of an implication for PPAR-γ, treatment with the PPAR-γ antagonist T0070907 had a similar effect (Supplementary Fig. 9C). In addition, BMDM treated with the PPAR-γ agonist Troglitazone significantly inhibited 25-HC ability to prevent the induction of “M2-like” BMDM by the TCM (Fig. 7B), establishing a direct link between the mode of action of 25-HC and PPAR-γ in TCM-exposed macrophages. More importantly, TCM-exposed, 25-HC treated, BMDM pretreated with Troglitazone maintained their ability to inhibit effector T cell functions and to promote T cell exhaustion when incubated with 25-HC (Fig. 7C). In vivo, LEC^{WT} mice transplanted with B16F10-OVA VEGF-C tumor cells mixed with WT BMDM controlled significantly better the growth of tumors upon OVA+CpG-B vaccination compared to LEC^{ΔCh25h} mice (Fig. 7D). In contrast, both LEC^{WT} and LEC^{ΔCh25h} mice efficiently controlled tumor growth after vaccination when tumor cells were mixed with PPAR-γ deficient macrophages (Fig. 7D), indicating that the lack of LEC-derived 25-HC can be compensated by the absence of PPAR-γ expression by tumor-associated myeloid cells.

Altogether, these experiments demonstrate that 25-HC produced by LECs in B16F10-OVA VEGF-C tumors prevents the induction of immunosuppressive functions in macrophages by the TME by

inhibiting their expression of PPAR-γ, consequently allowing effector T cells to maintain their effector phenotype in tumors and to provide better control of tumor growth.

Discussion

During tumor development, malignant cells take advantage of multiple mechanisms to evade immune-mediated recognition and killing⁵⁴. This is why approaches aiming at reinvigorating anti-tumor immunity currently represent the most promising treatment against cancer. The link between tumor-associated lymphangiogenesis and cancer cell spreading, and metastasis is well-established. However, the growth and the remodeling of LVs at the primary tumor, draining LNs and distant premetastatic niches, has been shown to not only support metastasis but also impact anti-tumor immunity⁵. Complex interactions between tumor cells, immune cells, and stromal cells make it hard to precisely decipher the contribution of LECs in shaping immune cell phenotype and functions in tumors. In addition, the plasticity of LECs and their response to molecular cues from the TME are still unclear.

Here we show that in comparison to LECs in steady-state skin or LNs, LECs in murine lymphangiogenic melanoma upregulate the oxysterol-producing enzyme Ch25h, which has been shown to play important roles in regulating lipid metabolism, gene expression, and immune activation. We further translated our findings to human tumors, showing that VEGF-C^{high} human melanoma cells promote LV expansion in immune-compromised mice, and induce the upregulation of Ch25h in the TME compared to skin LECs, suggesting that LECs in tumors from melanoma patients will likely upregulate Ch25h and produce 25-HC in the TME. In agreement, LECs express Ch25h mRNA in melanoma tumors.

Specific genetic abrogation of Ch25h in murine LECs demonstrates that in lymphangiogenic melanoma, LECs significantly contribute to the levels of extracellular 25-HC, the main product of the enzyme, which is beneficial for the control of tumor growth, by promoting anti-tumor immunity and response to immunotherapy. We further showed an impaired control of tumor growth of poorly lymphangiogenic tumors, and of different cancer types, in mice in which Ch25h was abrogated in LECs, indicating that beneficial Ch25h expression by LECs is not restricted to melanoma or to VEGF-C overexpressing tumors. The role of oxysterols in tumor settings is controversial. Some oxysterols (22-HC and 24-HC) can recruit pro-tumoral CXCR2⁺ neutrophils, promoting an immunosuppressive TME⁵⁵. Intracellular cholesterol and derivatives, including oxysterols, are directly sensed by LXRα/β nuclear receptors, leading to the transcription of genes implicated in reverse cholesterol transport. LXRs activation correlates with the generation of anti-inflammatory macrophages and DCs^{56,57}. In contrast, therapeutic GW3965 agonist-mediated LXR activation has been shown to promote anti-tumoral immune response, decreasing MDSC numbers while enhancing the activation of CTLs in both murine models and in cancer patients⁵⁸. However, we do not foresee LXRs activation as a pathway being involved in the ability of LEC-derived 25-HC to promote anti-tumor immunity. Indeed, LXRs sense intracellular cholesterol derivatives, whereas we show that tumor LECs do not exhibit any significant transcriptomic changes in the absence of Ch25h expression. In agreement, our in vitro and in vivo

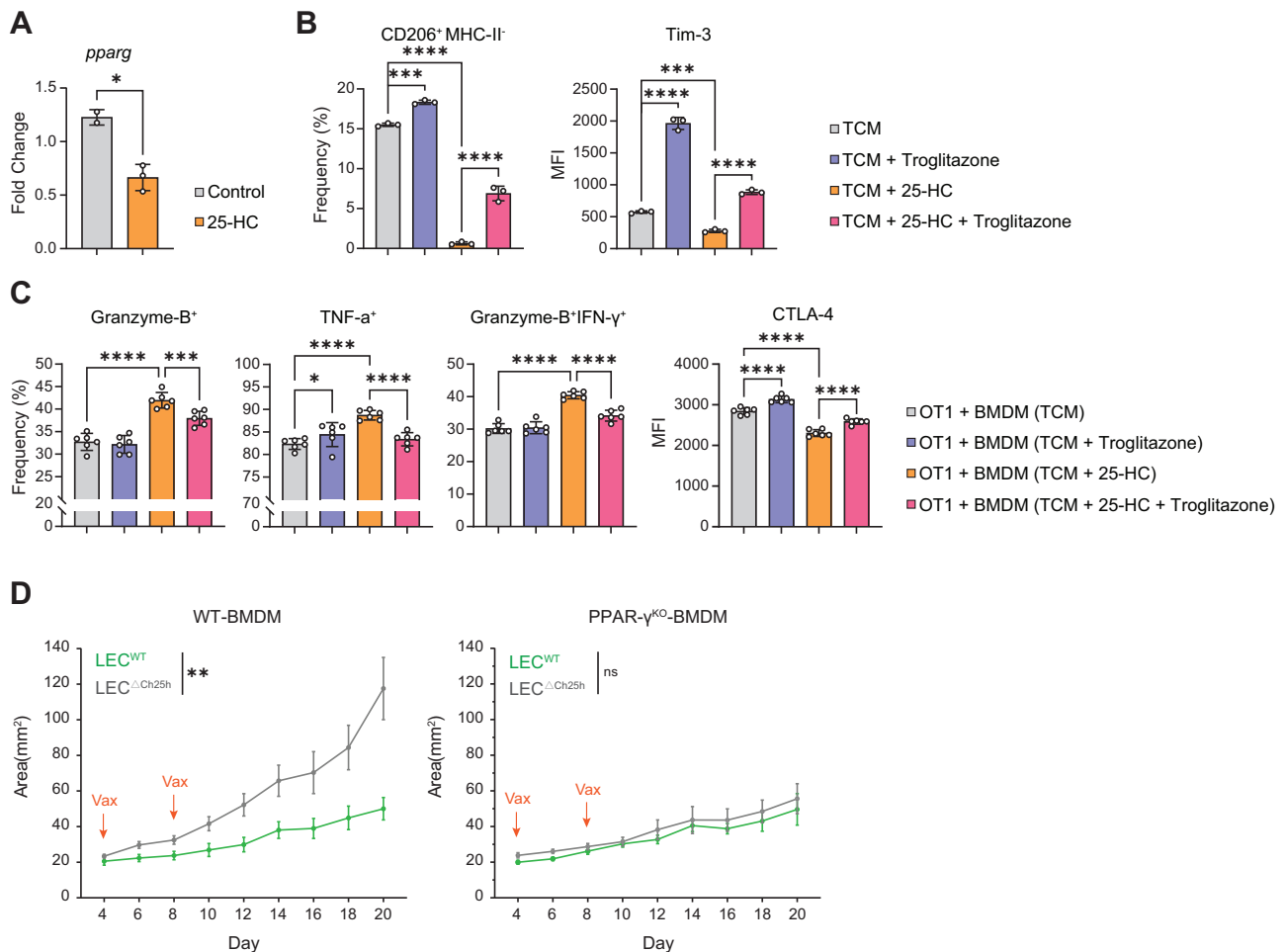


Fig. 7 | LEC-derived 25-HC dampens the immunosuppressive functions of tumor-associated macrophages by inhibiting PPAR- γ expression. **A** BMDM were incubated with B16F10-OVA VEGF-C tumor-conditioned medium (TCM), treated or not with 25-HC for 48 h, and analyzed by Q-PCR for PPAR- γ mRNA levels. Data were representative of two experiments with $n = 2-3$ replicates each. Data were presented as mean values \pm SD. Two-tailed unpaired t -test. * $P < 0.05$. **B** BMDMs were incubated with tumor-conditioned medium (TCM), treated or not with 25-HC, Troglitazone, or the combination of 25-HC and Troglitazone for 48 h. BMDM phenotype was analyzed by flow cytometry. Data were representative of two independent experiments with $n = 3$ replicates each. Data were presented as mean values \pm SD. One-way ANOVA. **** $P < 0.0001$; *** $P < 0.001$. **C** TCM-exposed BMDM

were treated or not with 25-HC, Troglitazone, or the combination of 25-HC and Troglitazone for 48 h, washed, and incubated with OT-1 effector cells for 48 h. T-cell phenotype was analyzed by flow cytometry. Data were representative of two independent experiments with $n = 6$ replicates each. Data were presented as mean values \pm SD. One-way ANOVA. * $P < 0.05$; *** $P < 0.001$; **** $P < 0.0001$. **D** LEC ^{Δ Ch25h} and LEC^{WT} mice were inoculated with B16F10-OVA VEGF-C cells mixed with either WT or PPAR- γ deficient (PPAR- γ ^{KO}) BMDM and vaccinated with OVA protein and CpG-B on day 4 and day 8. Tumor growth was followed. Data are presented as mean values \pm SEM. Two-way ANOVA, ** $P < 0.01$. Data were representative of two independent experiments with $n = 4-5$ mice/group each.

data show that 25-HC in the TME enhances the ability of macrophages to control tumor growth independently of the LXR pathway.

Whereas Ch25h has been described to be expressed by CTL and DCs in mouse tumors, including B16F10 melanoma^{18,46}, we could not detect it in lymphangiogenic B16F10-OVA VEGF-C tumors. This could be explained by the fact that the production of tumor-derived factors^{18,46}, which seem to inhibit Ch25h expression in both CTLs and DCs, might be increased in our model. Although we detected high levels of Ch25h expression in tumor-associated macrophages, it is likely that they do not dominantly contribute to extracellular 25-HC levels, as, at least in vitro, they do not release 25-HC in the extracellular medium, whereas LECs and BECs can do so. Although we did not decipher the mechanisms, it is likely that ECs exhibit particular features, which are not shared by macrophages, involved in the ability to secrete 25-HC. In addition, Ch25h abrogation in LECs leads to a significant decrease in extracellular 25-HC levels in tumors. It was recently shown that 25-HC produced by macrophages promotes their immunosuppressive phenotype in mouse colorectal cancer⁵⁹. Although this seems to be in contradiction with our data, it is possible that

extracellular and intracellular 25-HC differentially impact tumor-associated macrophage (TAM) phenotype and function. In their study, in vitro treatment of macrophages with 25-HC surprisingly promotes their immunosuppression. However, macrophages were pretreated with 25-HC before being exposed to IL-4 and IL-13, which might affect the data. It is however difficult to explain why the authors observed a better control of tumor growth in mice fully deficient for Ch25h, and why they reported a negative impact of high Ch25h expression in human colorectal cancer on prognosis, as we and others show the opposite¹⁵⁻¹⁷.

We observed that Ch25h is also expressed by tumor BECs, likely, as previously described, dampening their expansion and subsequent angiogenesis, and inhibiting metastasis¹⁵. However, as LECs seem to significantly contribute to extracellular 25-HC levels in lymphangiogenic melanoma, our data argue for an intracellular role of Ch25h expression and 25-HC in BECs in regulating the tumor-associated blood vasculature, whereas LEC-derived 25-HC certainly exerts extracellular functions. It was shown that in tumor-associated BECs, intracellular 25-HC prevents their uptake of TEVs, leading to their activation

and enhancing their ability to promote metastasis¹⁵. However, it is unlikely that this process occurs in tumor LECs, as the transcriptome of Ch25h deficient LECs exhibits high similarity with control LECs.

Our data show that in the absence of 25-HC production by LECs in tumors, infiltrating monocytes and macrophages adopt a completely different phenotype, with profound transcriptomic alterations, including a dampening of pro-inflammatory gene signature and an upregulation of genes implicated in immunosuppression. These modulations result from an unbalance of pathways that are important for myeloid cell functions, with impaired inflammatory response, TNF- α and IFN- γ response, or ROS production, and in contrast enhanced immunoregulation, M2-like responses, oxidative metabolism, and fatty acid oxidation. Interestingly, among the genes that are downregulated in monocytes and macrophages when 25-HC production by LECs has been abrogated, we identified IL-1 β . This can be surprising, since 25-HC has been shown to downregulate IL-1 β in macrophages¹². The study indicates that intracellular 25-HC acts as an antagonist of SREBP in the cytoplasm of macrophages, and therefore dampens their production of IL-1 β . However, our data show that 25-HC is produced by LECs extracellularly in the TME and promotes anti-tumoral macrophages and monocytes, including upregulation of IL-1 β . The role of IL-1 β in tumors is controversial. It has been described as a protumoral factor in most cancers^{60–63}, promoting M2-like macrophages and pro-tumoral neutrophil recruitment. However, and supporting our data indicating that 25-HC exposed macrophages promote anti-tumor effector T cell functions, it has been shown that IL-1 β enhanced the ability of tumor-specific T cells to eradicate established B16 melanoma⁶⁴. In the breast cancer model as well, IL-1 β promotes the infiltration of anti-tumor immune cells and controls primary tumor growth⁶⁵.

We further demonstrate that tumor-infiltrating myeloid cells are the primary targets of LEC-derived 25-HC. Indeed, myeloid cell depletion abolished the impact on effector T cell responses observed in the absence of Ch25h expression by LECs, indicating that T cells are not directly impacted by 25-HC released by LECs in the TME. A study has described that IL-27-induced Ch25h in CD4⁺ T cells acts as an immunoregulatory enzyme, through the production of 25-HC, interfering with cholesterol metabolism and leading to bystander CD4⁺ T cell inhibition⁶⁶. However, in the TME of the different models used, we could not detect Ch25h expression in T cells, suggesting that this pathway is not involved.

We provide additional *in vitro* and *in vivo* evidence that 25-HC can inhibit CD206⁺ immunosuppressive monocytes and macrophages. However, this effect is not sufficient to induce pro-inflammatory iNOS⁺ myeloid cells. *In vitro*, iNOS induction in macrophages requires pro-inflammatory polarizing cytokines (IFN- γ) and is potentiated by the addition of 25-HC. *In vivo*, iNOS expression by tumor macrophages and monocytes also requires T-cell derived cytokines (likely IFN- γ as well), as demonstrated by an almost total absence of iNOS⁺ myeloid cells in tumors in Rag2^{KO} mice, and is further potentialized by LEC-derived 25-HC. Therefore, 25-HC produced by LECs in the TME dampens myeloid cell immunosuppressive properties and further synergizes with other factors to promote pro-inflammatory myeloid cells and support anti-tumor effector T cells. These effects are amplified when the immunogenicity of the TME is boosted through immunotherapy protocols, such as vaccination or adoptive T cell transfer, and correlate with enhanced Ch25h expression by LECs in the TME. Our findings are in line with a study showing a role for 25-HC acting as an amplifier of inflammatory signaling in macrophages in the context of viral infection¹³. Although the molecular mechanism promoting the upregulation of Ch25h by LECs was not deciphered here, our data argue for a primary role of non-immune cells, either tumor cells themselves or stromal cells, and show that it is further promoted by vaccine-induced inflammation. Therefore, protocols aiming at strengthening tumor-specific immunity might boost the production of 25-HC by LECs in tumors and function as a loop to further enhance anti-tumor

immunity. Accordingly, we observed that melanoma patients with high Ch25h expression exhibit better survival and improved response to immunotherapy. This suggests that Ch25h expression might be a prognostic biomarker in melanoma patients and their response to immunotherapy. Further reinforcing the translational aspects of our findings, intratumoral injection of 25-HC redirects myeloid cells toward a less immunosuppressive phenotype, allowing a better control of tumor growth. However, the hydrophobic features of 25-HC may limit its direct use as a therapeutic compound.

Among the mRNA transcripts differentially regulated in macrophages and monocytes in the absence of *ch25h* expression by LECs, one particularly caught our attention, *pparg*. PPAR- γ belongs to the family of Peroxisome proliferator-activated receptors (PPARs), which are ligand-regulated transcription factors influencing several cellular pathways⁵². It has been known for decades that PPAR- γ agonists suppress the production of inflammatory cytokines by monocytes *in vitro*⁶⁷. Furthermore, PPAR- γ activation has been shown to modulate macrophage polarization *in vitro*, by suppressing their immunogenic state with downregulation of *nos2*, *tnf*, *il6*, *il1b*, and *mcp1*⁶⁸ while promoting their expression of immunosuppressive markers such as *il10*, *arg1*, *mrcl*, and others⁶⁹. In lymphangiogenic melanoma, we observed that both monocytes and macrophages upregulate *pparg* when LECs do not express Ch25h, likely promoting their immunosuppressive phenotype. *In vitro*, *pparg* is downmodulated by 25-HC in macrophages, supporting a direct implication of this pathway in controlling their immunoregulatory functions in tumors. The pathway is also implicated *in vivo*, with a restored control of B16F10-OVA VEGF-C tumor growth in LEC Δ Ch25h mice vaccinated with OVA+CpG-B when macrophages do not express PPAR- γ . Altogether, our data argue for a key role of LEC-derived extracellular 25-HC in dampening PPAR- γ expression and the immunosuppressive phenotype of monocytes and macrophages in the TME.

Because tumor LEC exhibits timely-related pro- and anti-tumorigenic effects, it is becoming clearer that it will be very difficult to target the whole lymphatic vasculature in tumors as a therapeutic approach. On the one hand, we and others have shown that LECs in primary tumors and in TdLNs can specifically inhibit tumor-specific T cells by functioning as MHCI and MHCII-restricted antigen-presenting cells to induce CD8⁺ T cell deletion and Treg generation, respectively^{67,19}. As such, it appears relevant to delete them, either through depleting antibodies or AAVs^{8,70,71}, or through immunotherapeutic approaches, such as their antigen-specific killing mediated by high-density tumor-infiltrating CTLs⁷². However, tumor LVs are needed for the drainage of tumor antigens and the migration of DCs to the TdLNs, and, therefore, are essential in the initiation of anti-tumor adaptive immunity^{73–75}. In addition, tumoral LVs increase the overall recruitment of immune cells in tumors⁸ and are therefore beneficial for immunotherapy protocols that either boost or reinvigorate immune cells^{8–10}. Therefore, the targeting of specific LEC functions, and not of the whole lymphatic vasculature, seems more pertinent, especially if it can be achieved through established immunotherapeutic protocols. Here we show that Ch25h upregulation by LECs in murine melanoma leads to the production of 25-HC in the TME and inhibits PPAR- γ in myeloid cells, allowing their conversion into pro-immunogenic cells that support T cell effector functions and prevent their exhaustion. Interestingly, this mechanism is amplified upon vaccination with a tumor antigen or after the adoptive transfer of anti-tumor effector T cells, with increased Ch25h expression in tumor LECs, increased pro-immunogenic myeloid cell generation, improved anti-tumor effector T cell responses and better control of tumor growth. Hence, besides their purpose of promoting anti-tumor immunity, immunotherapy protocols can further act on multiple LEC immunomodulatory facets, by favoring either their immunosuppressive^{6,7}, or their immunogenic functions, such as the upregulation of Ch25h. Altogether, these studies revealed the

incredible complexity of LEC-mediated immunomodulation, and indicate that the immunogenicity of the TME, which also depends on the course of tumor growth, greatly influences LEC phenotype and functions.

In our study, 25-HC produced by LECs in the TME has a beneficial effect on murine melanoma growth and response to immunotherapy, revealing an important role of extracellular oxysterols in preventing the polarization of tumor-associated monocytes and macrophages into immunosuppressive cells by inhibiting PPAR- γ . Therefore, an angle of attack, in combination with immunotherapy, would be to provide sufficient levels of tumoral extracellular 25-HC or to locally inhibit PPAR- γ .

Methods

Mice

C57BL/6N wild-type (WT) mice (*Mus musculus*, mixed sexes, 7–12 weeks old) were purchased from Charles River. Ch25h-eGFP^{fl/fl} mice were generated by Cyagen as published²⁰. Briefly, a constitutive Knock-In (KI) with conditional knockout (KO), using a floxed-reporter *Ch25h* knock-in, with eGFP was used as a reporter protein fused to the 3' end of *Ch25h*. The entire gene was further flanked with LoxP sites, avoiding promoter disruption. Linker-eGFP reporter was inserted in the targeting cassette and is thus not expressed as a fusion protein before cre-recombination. To generate mice selectively lacking Ch25h in lymphatic endothelial cells (LEC Δ Ch25h), Ch25h-eGFP^{fl/fl} mice were crossed with Prox1-Cre^{ERT2} mice²³. Ch25h-eGFP^{fl/fl} mice were used as controls (LEC^{WT}). For some experiments, LEC Δ Ch25h and LEC^{WT} mice were crossed on NSG or Rag2^{KO} mice (both obtained from Charles River). EBi2^{KO} mice were obtained from Prof. C. Pot. OVA₂₅₇₋₂₆₄-specific TCR transgenic OT-1 CD45.1 mice, CD45.1(Ly5), and C57BL/6 mice (obtained from Charles River), were bred in our animal facility. LXR-KO mice⁷⁶ and Vav-Cre PPAR- γ ^{fl/fl} mice⁷⁷ were described before. Ch25h full knockout mice were purchased from Jackson Laboratories. All mice were used between 6–12 weeks of age, randomized among groups, and maintained under SPF conditions at the animal facility of Geneva Medical School. Mice were housed under a 12 h:12 h light:dark schedule, with temperature maintained between 20 and 22 °C and a humidity level of around 50%. Mice had access to food and water ad libitum. No statistical methods were applied a priori to calculate group sample size, all experiments were performed at least twice with a minimum of three animals per group. All procedures were approved and performed in accordance with the guidelines of the animal research committee of Geneva (Commission Cantonale pour les Expériences sur les Animaux (CCEA) and the Office fédéral de la santé alimentaire et des affaires vétérinaires (OSAV)) under the licence numbers GE/149/19 and GE167.

Tamoxifen treatment

LEC Δ Ch25h mice and LEC^{WT} littermate control mice were injected intraperitoneally with tamoxifen (T5648, Sigma-Aldrich), 1 mg/mouse twice a day for 4 continuous days. Mice were used for experiments two weeks after the last injection.

Cell lines

Mouse B16F10 melanoma cells (ATCC) were transfected with ovalbumin (gift of B. Huard) (B16F10-OVA), and B16F10-OVA were engineered to overexpress VEGF-C (B16F10-OVA VEGF-C) as published¹⁹, and B16F10 and B16F10-OVA VEGF-C were maintained in RPMI supplemented with 10% heat-inactivated FBS, 100 μ M penicillin-streptomycin. Geneticin was added after 1 day of culture to select OVA-expressing cells. MC38 cells, MC38 VEGF-C cells⁷², E0771 cells, were maintained in DMEM (Gibco), 10% heat-inactivated FCS, 100 μ M penicillin-streptomycin. Cell lines were not authenticated, used at below passage 20, and tested negative for Mycoplasma. Human melanoma cell lines T1015, T362C, T618A, Me215, Me275⁷⁸, and T672E⁷⁹

were maintained in RPMI supplemented with 10% heat-inactivated FBS, 100 μ M penicillin-streptomycin. b.End3 mouse endothelial cells were a gift from B. Kwak.

Human melanoma samples

Patients signed the informed consent form for the translational clinical trial PEMSYS (NCT03534635) and agreed to the re-use of their biological material and clinical data. The study was approved by the competent local ethics committee (<https://www.cer-vd.ch/>, CER-VD, Switzerland) under the identification of BASEC ID 2017-01107.

Tumor cell inoculation and tumor measurement

Mice were anesthetized using isoflurane or a mix of Rompun 2% (Bayer)/Ketamine 10% (Vetoquinol) and their backs were shaved. Unless specified, 0.5×10^6 B16F10, B16F10-OVA VEGF-C, MC38, MC38 VEGF-C cells, and 2×10^6 human melanoma cell lines T362C and T618A cells, were injected in 100 μ l of PBS subcutaneously on the back dorsolateral side. For BMDMs and tumor cells co-injection experiment, 0.5×10^6 B16F10-OVA VEGF-C tumor cells were co-injected with 0.1×10^6 BMDMs from C57BL/6 mice or LXR-KO mice (OT-1 adoptive transfer experiment in NSG) or 0.25×10^6 BMDMs from WT/PPAR- γ ^{KO} mice (vaccination experiment) in 100 μ l of PBS subcutaneously on the back dorsolateral side. Primary tumor inoculation was controlled by measuring the distance between the front leg, the back leg, and the vertebral column of the mice, and the injection was always performed at the same distances from these three locations, at equal distance from the vertebral column and the back leg, representing -1/3 of the distance to the front leg. For orthotopic tumor models, 0.5×10^6 E0771 cells were injected into the fourth mammary fat pad, and 0.5×10^6 MC38 cells were injected into the rectum. Tumor size was monitored blindly every 1–2 days using a caliper, and tumor size was calculated by length \times width or measured at the ending point (weight). For some experiments, tumor growth has been normalized in order to pool data from different experiments. Tumor size for each day was normalized to the size of controls or to the size for each group from measurement at the first timepoint (details are indicated in the figure legends accordingly). Mouse exclusion criteria permitted by our ethics committee are tumor size >15 mm (diameter) and/or signs of pain or anxiety. We confirm that the exclusion criteria were not exceeded.

Tissue digestion and single-cell preparation

Stromal cell isolation. Tissues were cut into small pieces and digested in RPMI containing collagenase IV (1 mg/ml; Worthington Biochemical Corporation), DNase I (40 μ g/ml; Roche), and 1% FBS for 30 min at 37 °C. Samples were mixed up and down every 10 min. Tubes were centrifuged for a few seconds at 400 \times g, and supernatants were filtered through a 70 μ m cell strainer in FACS buffer to stop the reaction. The remaining tissue was further digested in RPMI with collagenase D (1 mg/ml; Roche), DNase I (40 μ g/ml; Roche), and 1% of FBS for 20 min at 37 °C, with an additional two cycles of repeated pipetting. The solution was filtered through a 70 μ m cell strainer in FACS buffer and pooled into the first collected tubes. For tumors, digestion was followed by debris removal using Lympholyte[®]-M (CEDARLANE) according to the manufacturer's instructions. For LNs, stromal cells were further enriched by CD45 negative selection using MACS[®] Column (Miltenyi Biotec). For skin, the remaining tissues after digestion were gently scratched on 70 μ m cell strainers and filtered for the following staining.

Leukocyte isolation. Tissues were cut into small pieces and digested in RPMI containing collagenase D (1 mg/ml; Worthington Biochemical Corporation), DNase I (40 μ g/ml; Roche), and 1% FBS for 40 min at 37 °C. Samples were mixed up and down every 10 min. The solution was filtered through a 70 μ m cell strainer in FACS buffer to stop the reaction. For tumors, digestion was followed by debris removal using

Lympholyte®-M (CEDARLANE) according to the manufacturer's instructions.

Mouse OT-1 T cell isolation, activation, and purification

Spleens and LNs from OT-1 CD45.1 mice were smashed, filtered through a 70- μ m mesh filter, and centrifuged at 400 \times g for 5 min. Red blood cells were lysed with ammonium-chloride-potassium lysis buffer. Following the addition of the cell culture medium, splenocytes were washed and resuspended in complete RPMI (supplemented with 10% FBS, 1% penicillin-streptomycin, and 50 mM 2- β -mercaptoethanol). OT-1 cells were activated with 1 nM OVA-1 peptide (SIINFEKL) (Sigma-Aldrich) in the presence of 100 U/ml interleukin-2 (IL-2) (PeproTech) in vitro for 3 days. Activated OT-1 T cells were purified by using a CD8⁺ T cell isolation kit (Miltenyi Biotec) according to the manufacturer's instructions.

Generation of naive bone marrow-derived macrophages (BMDMs)

Bone marrow cells were collected from femurs obtained from 8 to 10-week-old mice. After red blood cell lysis, bone marrow cells were seeded at a density of 10⁷ cells/100 \times 15-mm Petri dish and cultured at 37 °C in DMEM containing 20 ng/ml CSF1 (PeproTech). BMDMs were ready for use on day 7 following a fresh medium change on day 4.

Vaccination

B16F10-OVA VEGFC tumor-bearing mice were injected subcutaneously at days 4 and 8 post tumor inoculation with OVA protein (50 μ g/mice; Invivogen) and CpG-B 1826 (30 μ g/mice; Invivogen).

Activated OT-1 T cell adoptive transfer

OT-1 CD45.1 cells were activated and purified as described above. In the experiments with LEC^{WT} and LEC Δ ^{Ch25h} mice, B16F10-OVA VEGFC tumor-bearing mice received 1.5 \times 10⁶ activated OT-1 cells per mouse intravenously at day 8 post tumor inoculation. In the experiments with NSG, NSG-LEC^{WT}, and NSG-LEC Δ ^{Ch25h} mice, 0.5 \times 10⁶ activated OT-1 cells were injected intravenously at day 8 post tumor inoculation. Tumor growth was measured every 2 days using a caliper.

25-HC intratumoral injection

25-HC was resuspended into a solution of 50% Ethanol (Fluka Analytical) and 50% Poly (ethylene glycol) methacrylate-500 (Sigma) via sonication. 25-HC or control solution was injected intratumorally at 200 μ g in 20 μ l/mouse every two days starting at day 4 post tumor injection.

Bone marrow (BM) chimeric mice construction

Bone marrow (BM) chimeric mice were generated as described⁸⁰. Briefly, BM cells were recovered from the tibia and femurs of WT CD45.1⁺ and EBI2^{KO} CD45.1^{+/2+} donor mice and mixed in a 1:1 ratio. About 5–7 \times 10⁶ cells were injected intravenously into sub-lethally irradiated recipient LEC^{WT} and LEC Δ ^{Ch25h} mice (two consecutive doses of 500 cGy with 4-h intervals). Experiments were performed at least 6 weeks after reconstruction.

In vitro BMDM polarization and treatment with 25-HC or 7-keto-25-HC

BMDMs from WT or Ch25h^{-/-} mice were stimulated for 48 h with IFN- γ (20 ng/ml, PeproTech) or with IL-4 (50 ng/ml, PeproTech) to polarize toward an M1-like or M2-like phenotype, respectively, and treated or not with 1 μ g/ml of either 25-HC (MedChemExpress) or 7-keto-25-HC (Cayman Chemical Company)

Ex vivo LEC cultures

LNs were harvested and digested in MEM Alpha Medium (Gibco) with Dispase (800 μ g/ml, Sigma), Collagenase P (200 μ g/ml, Roche), DNase I

(100 μ g/ml; Roche) at 37 °C, resuspended every 10 min, 2/3 of the digestion mix was transferred to collecting tubes and replaced by fresh digestion mix. The operation was repeated until full digestion. Culture plates precoated with PureCol (10 μ g/ml, Advanced BioMatrix) and human fibronectin (10 μ g/ml, Gibco) were seeded with the cell suspension for 7 days. The medium, containing cells in suspension, was removed at day 1 and day 3, to keep adherent cells that are mainly a mixture of (CD45 negative) LECs and FRCs. LECs were sorted with a FACS Aria Fusion sorter (BD) based on CD45^{neg}GP38⁺CD31⁺ expression and put back in culture on precoated culture plates.

In vitro 25-HC release experiments

LECs and BMDMs were generated from WT and Ch25h knockout mice. 10,000 cells/well of LECs, BMDMs, and b.END3 cells were put in culture in 96-well plates precoated with PureCol (10 μ g/ml, Advanced BioMatrix) and human fibronectin (10 μ g/ml, Gibco) for LECs, and 1.5% gelatin for b.END3 cells. Cells were treated with B16-OVA VEGF-C cell culture supernatants for 3 days, and supernatants were harvested for 25-HC dosage.

In vitro BMDMs treatment with tumor conditional medium (TCM), 25-HC, 7-keto-25-HC, PPAR- γ inhibitor, and PPAR- γ agonist

BMDMs from WT, Ch25h^{-/-} or LXR-KO mice were harvested and pre-seeded into a Petri dish or six-well non-treated cell culture plates (Corning Inc.) overnight and treated with different compounds used either alone or in combination: 1 μ g/ml 25-HC (MedChemExpress), 1 μ g/ml 7-keto-25-HC (Cayman Chemical Company), 20 nM PPAR- γ inhibitor T0070907 (Cayman Chemical Company), 50 μ M PPAR- γ agonist Troglitazone (MedChemExpress) and TCM (prepared from 2 days B16F10-OVA VEGF-C cells in vitro culture medium). After 48 h, BMDMs were harvested for flow cytometry, Q-PCR, or co-culture experiments with T cells.

For in vitro co-culture of BMDMs and OT-1 cells, OT-1 cells and BMDMs were preactivated or pretreated as described above. Activated OT-1 cells and pretreated BMDMs were co-cultured at a ratio of 1:5 in flat-bottom 96-well plates in a complete RPMI medium. After 48 h, OT-1 cells were harvested for flow cytometry.

Lymphatic vessel drainage

Dextran-Alexa Fluor 488 (40 kD) was injected intratumorally (3 μ l at 100 mg/ml). 20 min later, inguinal and axillary tumor dLNs and their contralateral control LNs were harvested and dissociated in 200 μ l of PBS, centrifuged at 400 \times g and 100 μ l of supernatant from each sample was transferred to a new plate. A fluoro spectrometer (Spectamax Paradigm; Molecular Devices) was used to determine Alexa Fluor 488 fluorescence intensity in dLNs. The background of fluorescence in the contralateral side was removed to the intensity of the dextran-Alexa Fluor 488 tumor side.

Flow cytometry analysis

Monoclonal antibodies (mAbs) used for flow cytometry are listed in Supplementary Table 1. Unless specified, antibodies were used at 1:200 working dilution. For flow cytometry, single-cell suspensions were incubated with FcBlock (anti-CD16/32 Fc γ RII-RIII; Invitrogen) for 10 min, at 4 °C and stained for extracellular markers with antibodies and fixable viability dye (Dye eFluorTM 780, Thermo Fisher) for 20 min in PBS at 4 °C. To assess Ch25h-GFP expression, cells were stained for extracellular markers, and live-cell impermeant DNA DRAQ7 dye (Biolegend) was used for viability evaluation on unfixed cells. Anti-mouse antibodies used for stain cell surface markers: anti-GP38 (8.1.1), anti-CD31(390), anti-I-A/I-E (M5/114.15.2), anti-B220 (RA3-6B2), anti-CD11b (MI/70), anti-CD11c (HL3 or N48), anti-CD19 (6D5), anti-CD3 (REA641), anti-CD4 (GK1.5 or RM4-5), anti-CD45 (30-F11), anti-CD45.1 (A20), anti-CD45.2 (104), anti-CD8 (53-6.7), anti-CD86 (GL1), anti-F4/80

(BM8), anti-I-a/I-E (M5/114.15.2 or 2G9), anti-Ly6C (HK1.4), anti-Ly6G (1A8), anti-NK1.1 (PK136), anti-PD-1 (RMP1-30), anti-PD-L1 (10 F.9G2), anti-TCR β (H57-597), anti-Ter119 (TER-I19), anti-Tim-3 (RMT3-23), H-2K(b) chicken ova 257-264 SIINFEKL tetramer (NIH tetramer core facility). Intracellular staining was performed using the Intracellular Fixation & Permeabilization buffer set (eBioscience). Antibodies to intracellular markers: anti-CD206 (C068C2), anti-CD68 (FA-11), anti-Foxp3 (FJK-16s), anti-Granzyme-B (GB11), anti-IFN- γ (XMGL.2), anti-iNOS (CXNFT), anti-Ki67 (SolA15), and anti-TNF- α (MP6-XT22).

For IFN- γ , Granzyme-B, and TNF- α , cells were first re-stimulated in complete RPMI containing PMA (100 ng/ml; Sigma-Aldrich), Ionomycin (1 μ g/ml, Sigma-Aldrich), and Golgi Plug solution (1/1000; BD Biosciences), and incubated 4 h at 37 °C, 5% CO₂.

Data were acquired with a Fortessa analyzer (BD) and analyzed using FlowJo software (FlowJo).

Hematoxylin & Eosin (H&E) and immunofluorescence (IF) staining

Tumors and dLNs were embedded either into OCT (Optimal cutting temperature) medium and kept at -80 °C or fixed with 4% paraformaldehyde (PFA) and embedded into paraffin. Frozen samples were sectioned into 7 μ m, air-dried, and postfixed with 4% PFA for 10 min at room temperature (RT), washed with PBS three times, and followed with permeabilization with 0.1% Triton-100 for 10 min. Paraffin samples were sectioned into 4–7 μ m, di-paraffined, and performed antigen retrieval with the Tintorettriever pressure cooker (Bio SB) using the high-pressure setting for 10 minutes in Tris-EDTA buffer (pH 9) before the following steps.

H&E staining was performed with H&E staining kit (Vector Laboratories) for LN-metastasis analysis. Images were obtained by Axio Scan.Z1 (Zeiss), processed and analyzed with QuPath. Metastasis fraction was calculated as the percentage of melanoma area among total LN area.

IF staining was performed for lymphatic vessel density, and macrophage/monocyte proximity analysis. Following the blocking with 10% FBS for 1 h at RT. The sections were stained overnight with primary antibodies diluted in 10% BSA at 4 °C overnight. The following primary anti-mouse antibodies were used according to the experiments: anti-Lyve-1 (1:1000, ab14917, Abcam; 1:200, 14-0443-82, Invitrogen), anti-CD8 (1:100, 14-0808-82, Thermo), anti-CD68 (1:2000, 137002, Biolegend), anti-CD31 (1: 100, AF3628, R&D Systems), anti-Ch25h (1:100, ABIN1387938, ANTIBODIES). Sections were washed and stained with unconjugated secondary fluorochrome-coupled antibodies for 1 h at room temperature. The following secondary antibodies from Thermo were used: Alexa FluorTM546 goat anti-rat (LOT: 2146039), Alexa FluorTM488 goat anti-rabbit (LOT: 1386400), Alexa FluorTM647 donkey anti-rabbit (LOT: 2420695). Prior to mounting with FluoromountTM Aqueous Mounting Medium (Sigma), sections were stained with DAPI (1:1000 dilution of 1 mg/ml stock) for nuclei staining. Images were obtained by spinning disk confocal microscope (Axio Examiner Z1 Advanced Microscope Base, Zeiss) equipped with a confocal scanner unit CSU-X1 A1 (Yokogawa Electric Corporation). The fluorescence was detected using three laser-excitation wavelengths (488 nm, 561 nm, and 640 nm; Laser-Stack v4 Base, 3i) in combination with appropriate band-pass-emission filters (Semrock), an electron-multiplying charge-coupled device camera (EMCCD, Evolve 512 10 MHz Back Illuminated, Photometrics) and a 10x /0.3 NA water immersion objective (W Plan Aplanachromat, Zeiss). 3D image stacks were obtained by sequential acquisition of multiple fields of views along the z-axis using a motorized XY-stage (ProScan, Prior). SlideBook software (6.0.17, 3i) was used for image acquisition and the creation of maximum projections. The subsequent generation of montage images from contiguous positions was performed using the Fiji grid/collection stitching plugin⁸¹.

RNA in situ hybridization combined with immunofluorescence

For the combined RNA-ISH-IF (RNAscope[®]) analysis, samples were fixed in 4% NBF at 4 °C for 24 h and 5- μ m thick sections from FFPE blocks were cut. In situ hybridization (ISH) with co-immunostaining (IF) was performed following the manufacturer's recommendation of the RNAscope Multiplex Fluorescent Reagent Kit v2 assay (Cat# 323100, Advanced Cell Diagnostics). Standard conditions were used: 15 min. incubation for the Antigen retrieval step and 8 min. for Protease Plus treatment. Combined ISH and antibody staining with Opal dyes (Akoya Biosciences) was performed manually for ISH and employing an automated Ventana Discovery Ultra Staining module (Ventana, Roche) for IF. For the individual experiments, the following combinations of RNAscope[®] probes (all from Biotechne) and antibodies were employed. All opal dyes were purchased from Akoya Biosciences inc: Probe-Hs-CH25H probe (Cat# 533811) with opal570 (Cat# FP1488001KT), anti-Podoplanin Ab (Cat# 916605, Biolegend, diluted 1/250) with opal690 (Cat# FP1497001KT). Nuclei were visualized by final incubation with Spectral DAPI (1/10, Cat# FP1490, Akoya Biosciences). The slides were mounted with fluorescence mounting medium (Cat# S3023, Dako) and stored in the dark at 4 °C until scanned within 48 h. Images were acquired on the Vectra Polaris automated imaging system at 40X (Akoya Biosciences, Marlborough, USA), allowing the unmixing of spectrally overlapping fluorophores and tissue autofluorescence of whole slide scans using Phenochart (Akoya Biosciences).

RNA isolation and quantitative RT-PCR (Q-PCR)

Total RNA was isolated using Trizol Reagent (Thermo) or miRNeasy Mini Kit (Qiagen) depending on cell numbers. RNA quantity and quality were analyzed using a Nanodrop 2000 (Thermo Fisher) or Bioanalyzer (Agilent Technologies). Reverse transcription was performed using PrimeScript[™] RT Reagent Kit (Takara) followed by a pre-amplification of the respective genes of interest using the TaqMan Preamp Master Mix (Applied Biosystems) or M-MLV (Promega). Q-PCR analyses were performed with the ABI Prism 7900 HT detection system and the PowerUp SYBR Green Master Mix (Applied Biosystems). Primer sequences are provided in Supplementary Table 2. Quantification of the transcript was performed using the 2- $\Delta\Delta$ Ct method with glyceraldehyde phosphate dehydrogenase (*gapdh*), *actb*, or together with *rpl32* as internal reference genes.

Bulk RNA sequencing and data analysis

Single cell suspensions from tumors, LNs, and skin, were obtained as described above. Cells were stained with cell surface markers and live/dead dye DRAQ7 (Biolegend), and then sorted directly into RNA Protector Reagent (Qiagen) with a FACS Aria Fusion sorter (BD). For LECs from C57BL/6 NdLNs, TdLNs, and tumors, cells were sorted as CD45⁺CD31⁺GP38⁺ population from B16F10-OVA VEGF-C tumor-bearing mice sacrificed at day 11. For tumor LECs from LEC^{WT} and LEC Δ Ch25h mice, cells were sorted from tumors as CD45⁺CD31⁺GP38⁺ cells from B16F10-OVA VEGF-C tumor-bearing mice sacrificed on day 11. For macrophages and monocytes from LEC^{WT} and LEC Δ Ch25h mice, cells were sorted from tumors of OVA+CpG-B vaccinated B16F10-OVA VEGF-C tumor-bearing mice sacrificed at day 24. Sorting was based on common markers CD45⁺Lin (CD19/CD3)⁻Ly6G⁺CD11b⁺ with exclusion of DCs (CD11c^{hi} F4/80⁻), and further separated as macrophages (F4/80⁺Ly6C⁻) and monocytes (F4/80⁺Ly6C⁺).

Total RNA was quantified with a Qubit (fluorimeter from Life Technologies) and RNA integrity was assessed with a Bioanalyzer (Agilent Technologies). The SMART-Seq v4 kit from Clontech was used for the reverse transcription and cDNA amplification according to the manufacturer's specifications, starting with 1 ng (for LECs and Macrophages) or 10 ng (for monocytes) of total RNA as input. 200 pg of cDNA were used for library preparation using the Nextera XT kit from Illumina. Library molarity and quality were assessed with Qubit

and TapeStation using a DNA High-sensitivity chip (Agilent Technologies). Libraries were sequenced on a HiSeq 4000 (for LECs)/NovaSeq 6000 (for macrophages and monocytes) Illumina sequencer for SR50 (for LECs) or SR100 (for macrophages and monocytes) reads.

Analysis for LECs from C57BL/6 NdLNs, TdLNs, and tumors (GSE242026). FastQ reads were mapped to the ENSEMBL reference genome (GRCm38.80) using STAR version 2.4.0j⁸² with standard settings, except that any reads mapping to more than one location in the genome (ambiguous reads) were discarded ($m=1$). A unique gene model was used to quantify reads per gene. Briefly, the model considers all annotated exons of all annotated protein-coding isoforms of a gene to create a unique gene where the genomic region of all exons is considered coming from the same RNA molecule and merged. All reads overlapping the exons of each unique gene model were reported using featureCounts version 1.4.6-p1⁸³. Gene expressions were reported as raw counts and, in parallel, normalized in RPKM to filter out genes with low expression values (1 RPKM) before calling for differentially expressed genes. Library size normalizations and differential gene expression calculations were performed using the package edgeR⁸⁴ designed for the R software. Only genes having a significant fold-change (Benjamini–Hochberg corrected p value <0.001) were considered. Sample similarity was analyzed as follows: Euclidean distance between samples was calculated from the log transformed gene expression counts matrix with the dist function (vectors), 0 = identity (same sample). The color key indicates the values given by the Euclidean distance calculation.

Analysis for TA-LECs from LEC^{WT} and LEC^{ΔCh25h} mice (GSE242150). Mapping was done with the STAR v.2.7.0 software to the UCSC mm10 Mus musculus reference. Biological quality control and summarization were done with PicardTools (v.1.141). The number of reads was prepared with HTSeq v0.9.1 (htseq-count). The differential expression analysis was performed with R/Bioconductor package EdgeR (v.3.26.8). The genes having a count above 1 count per million reads (cpm) in at least 3 samples were kept for the analysis. The poorly or not expressed genes were filtered out. The filtered dataset consists of 13,454 genes. The differentially expressed gene tests were done with a GLM (general linear model) with a negative binomial distribution. The differentially expressed genes p values are corrected for multiple testing errors with a 5% FDR (false discovery rate). The correction used is Benjamini–Hochberg (BH). The likelihood test was used for the statistical test of differential expression.

Analysis for macrophages and monocytes from LEC^{WT} and LEC^{ΔCh25h} mice (GSE239972). Mapping and quantification using STAR and Salmon: nf-core/rnaseq pipelin (v.3.9) on mm10. Counts were normalized for library size using the TMM method from EdgeR (v.3.32.1) and voom from limma (v.3.46.0). Differential expression was computed with limma, after filtering out low expressed genes (with average FPKM <2 or average reads counts <5) and not characterized, non-coding or pseudo genes; the filtered set of genes contains $n=9392$ genes. Gene set enrichment analysis was performed with clusterProfiler (v3.18.1) applying GSEA (Gene Set Enrichment Analysis) on the Hallmark collection of genesets. The gene lists used for M1 and M2 signature enrichment were used as described in ref. 50. Gene lists for heatmaps are listed in Supplementary Table 3.

Generation of anti-CSF1R(CD115) depleting antibody

Monoclonal anti-mouse CSF1R(CD115) depletion antibody was generated with AFS98 hybridoma. Briefly, AFS98 hybridoma cells were cultured with the CELLline 1000 system (Wheaton) in PFHM-II medium supplementing with 1% penicillin and streptomycin. Cell culture content was harvested on day 14 and day 21. Hybridoma cells were spined down by centrifuging at $400\times g$ for 5 min. The supernatant was

harvested, filtered, and concentrated (using AMICON concentrators) for purification (performed by our Protein Core Facility). Antibodies were purified with Superdex200 10/300 Size Exclusion Chromatography (SEC) system. The purity of the antibodies was analyzed by acrylamide gel electrophoresis.

In vivo myeloid cell depletion

To deplete myeloid cells in the vaccination experiment, 1 mg/ mouse anti-CSF1R depletion antibody or PBS control was injected intraperitoneally at day 10 (2 days after second dose of vaccination) after tumor inoculation. In the non-vaccinated experiment, 1 mg/ mouse anti-CSF1R depletion antibody or PBS was injected intraperitoneally on day 4 after tumor inoculation. The following injections were done every 3 days at 500 $\mu\text{g}/\text{mouse}$ until the day of sacrifice for all experiments.

In vivo B-cell depletion

To deplete B cells in the B16F10-OVA VEGFC model, one dose of 250 $\mu\text{g}/\text{mouse}$ anti-CD20 depletion antibody was injected intraperitoneally 3 days before tumor inoculation.

Correlation analysis in TCGA melanoma dataset

A Spearman's correlation analysis was carried out between CH25H gene expression and a signature of lymphatic vessels (LV signature 1: *pdpn*, *vegfc*, *lyve1*; LV signature 2: *prox1*, *flt4*, *lyve1*, *pdpn*, *vegfc*) or M1/M2 macrophage (Blueprint 2) signatures in The Cancer Genome Atlas' (TCGA) skin cutaneous melanoma (SKCM) patients' dataset ($n=458$ patients), accessed via the UCSC Xena project (<http://xena.ucsc.edu>). Correlation between CH25H and M1/M2-signature in normal skin samples was performed in TCGA normal skin and normal skin from the GTEx dataset, both sun-exposed and non-exposed. Different datasets and analysis workflows were used as described^{21,85}. All tests were two-sided and without adjustments for multiple comparisons.

Survival analyses in the TCGA melanoma dataset

Survival analysis was carried out using CH25H gene expression in the TCGA melanoma dataset. We accessed patient OS or PFS durations and tumor gene expression profiles for SKCM patients' dataset ($n=458$) based on the UCSC Xena project (<http://xena.ucsc.edu>)²¹. Briefly, OS/PFS analysis was based on a log-rank hypothesis test (the Mantel–Cox statistical test) that also estimated the Cox-proportional hazard ratio (HR) and the 95% confidence intervals accompanied by a Kaplan–Meier (KM) plot. Herein, the expression threshold cut-off at 25% (top) vs. 75% (rest) gene expression level was used for splitting the patients into high-expression and low-expression sub-cohorts. All tests were two-sided and without adjustments for multiple comparisons.

Survival analysis of immuno-oncology clinical trials

Patient survival analysis in immuno-oncology clinical trials was carried out using *ch25h* gene expression. We accessed tumor transcriptomic data from melanoma patients profiled before anti-PD-1 immunotherapy alone, anti-CTLA-4 immunotherapy alone, or a combination of anti-PD-1/CTLA-4 immunotherapy. These data and subsequent OS estimates were accessed from an integrated dataset of multiple clinical trial studies consisting of 570 melanoma patients^{21,22,86}. Briefly, OS analysis was based on a log-rank hypothesis test (the Mantel–Cox statistical test) that also estimated the Cox-proportional hazard ratio (HR) and the 95% confidence intervals accompanied by a Kaplan–Meier (KM) plot. Herein, the expression threshold cut-off was based on a statistical auto-cutoff criterion^{21,85,87}. Thresholds (overall expression ranges lowest–highest) for each treatment condition: PD1: 8 (1–1571); CTLA-4: 29 (2–283); PD1 + CTLA-4: 29 (2–80). All tests were two-sided and without adjustments for multiple comparisons.

Ex vivo and in vitro 25-HC and 7-keto-25-HC dosage

25-hydroxycholesterol was analyzed using a validated HPLC-MS method⁵⁸⁴. For tumor interstitial fluid: harvested tumors were placed on 70 µm filters at the top of 5-ml-tubes, and centrifuged at 300×g for 20 min, interstitial fluid was collected. For serum samples: fresh blood was collected and centrifuged at 500×g for 5 min, and serum was collected. For in vitro samples: LECs, BMDMs, and b.End3 blood endothelial cells were treated with tumor cell supernatants for 3 days, supernatant were harvested and centrifuged at 500×g for 5 min to remove the debris. Tumor interstitial fluids and sera were collected and placed in glass vials containing d₇-4β-hydroxycholesterol and d₇-24-hydroxycholesterol as deuterated internal standards and dichloromethane (8 ml), methanol (4 ml, containing 10 µg of butylated hydroxytoluene), and water (2 ml, containing 20 ng ethylenediamine-tetraacetic acid). The samples were then mixed and sonicated. After that, they were centrifuged, and the organic phase was recovered and dried under nitrogen steam. Finally, samples were purified by solid-phase extraction using columns made of normal silica. Cholesterol was removed from the samples using hexane-isopropanol (99:1, v/v). 25-HC (from tumor interstitial fluid and sera) and 7-keto-25-HC (from tumor interstitial) were then eluted using hexane-isopropanol (7:3, v/v) and analyzed by HPLC-MS using an LTQ-Orbitrap XL mass spectrometer (Thermo Fisher Scientific) coupled to an Accela HPLC system (Thermo Fisher Scientific). Chromatographic separation was performed using an Ascentis Express C18 column (2.7 µm, 150 × 4.6 mm, Sigma), kept at 15 °C. The mobile phase was a gradient of methanol and water containing acetic acid. Values have been normalized to the sample volume.

Statistical analysis

Data were analyzed using Prism 9 software (GraphPad). Unless specified, analysis for significance was performed by one-way or two-way ANOVA when more than two groups were compared and by two-tailed Student *t*-test when only two groups were compared. *p* < 0.05 was considered statistically significant (**p* < 0.05, ***p* < 0.01, ****p* < 0.001, *****p* < 0.0001).

Reporting summary

Further information on research design is available in the Nature Portfolio Reporting Summary linked to this article.

Data availability

The data underlying this article are accessible at <https://doi.org/10.26037/yareta:aoweiaahjvcjmjmf23mdtefyu>. All data needed to evaluate the conclusions in the paper are present in the paper and/or the Supplementary Materials. The RNA sequencing data generated in this study has been deposited in the Gene Expression Omnibus (GEO) database with public accessibility, the link to each dataset is listed below: Bulk RNA sequencing on LECs from C57BL/6 NdLNs, TdLNs, and tumors (GSE242026): <https://www.ncbi.nlm.nih.gov/geo/query/acc.cgi>. Bulk RNA sequencing on TA-LECs from LEC^{WT} and LEC^{ΔCh25h} mice (GSE242150): <https://www.ncbi.nlm.nih.gov/geo/query/acc.cgi>. Bulk RNA sequencing on macrophages and monocytes from LEC^{WT} and LEC^{ΔCh25h} mice (GSE239972): <https://www.ncbi.nlm.nih.gov/geo/query/acc.cgi> Source data are provided with this paper.

References

- Jones, D., Pereira, E. R. & Padera, T. P. Growth and immune evasion of lymph node metastasis. *Front. Oncol.* **8**, 36 (2018).
- Stacker, S. A. et al. Lymphangiogenesis and lymphatic vessel remodelling in cancer. *Nat. Rev. Cancer* **14**, 159–172 (2014).
- Hirakawa, S. et al. VEGF-A induces tumor and sentinel lymph node lymphangiogenesis and promotes lymphatic metastasis. *J. Exp. Med.* **201**, 1089–1099 (2005).
- Qian, C. N. et al. Preparing the “soil”: the primary tumor induces vasculature reorganization in the sentinel lymph node before the arrival of metastatic cancer cells. *Cancer Res.* **66**, 10365–10376 (2006).
- Garnier, L., Gkoutidi, A. O. & Hugues, S. Tumor-associated lymphatic vessel features and immunomodulatory functions. *Front. Immunol.* **10**, 720 (2019).
- Gkoutidi, A. O. et al. MHC class II antigen presentation by lymphatic endothelial cells in tumors promotes intratumoral regulatory T cell-suppressive functions. *Cancer Immunol. Res.* **9**, 748–764 (2021).
- Lane, R. S. et al. IFNγ-activated dermal lymphatic vessels inhibit cytotoxic T cells in melanoma and inflamed skin. *J. Exp. Med.* **215**, 3057–3074 (2018).
- Fankhauser, M. et al. Tumor lymphangiogenesis promotes T cell infiltration and potentiates immunotherapy in melanoma. *Sci. Transl. Med.* <https://doi.org/10.1126/scitranslmed.aal4712> (2017).
- Sasso, M. S. et al. Lymphangiogenesis-inducing vaccines elicit potent and long-lasting T cell immunity against melanomas. *Sci. Adv.* <https://doi.org/10.1126/sciadv.abe4362> (2021).
- Song, E. et al. VEGF-C-driven lymphatic drainage enables immunosurveillance of brain tumours. *Nature* **577**, 689–694 (2020).
- Mao, S. et al. Studies in the antiviral molecular mechanisms of 25-hydroxycholesterol: disturbing cholesterol homeostasis and post-translational modification of proteins. *Eur. J. Pharm.* **926**, 175033 (2022).
- de Freitas, F. A. et al. Effects of oxysterols on immune cells and related diseases. *Cells* <https://doi.org/10.3390/cells11081251> (2022).
- Gold, E. S. et al. 25-Hydroxycholesterol acts as an amplifier of inflammatory signaling. *Proc. Natl Acad. Sci. USA* **111**, 10666–10671 (2014).
- Kloudova, A., Guengerich, F. P. & Soucek, P. The role of oxysterols in human cancer. *Trends Endocrinol. Metab.* **28**, 485–496 (2017).
- Lu, Z. et al. Regulation of intercellular biomolecule transfer-driven tumor angiogenesis and responses to anticancer therapies. *J. Clin. Invest.* <https://doi.org/10.1172/JCI144225> (2021).
- Ortiz, A. et al. An interferon-driven oxysterol-based defense against tumor-derived extracellular vesicles. *Cancer Cell* **35**, 33–45.e36 (2019).
- Lu, Z. et al. ATF3 and CH25H regulate effector trogocytosis and anti-tumor activities of endogenous and immunotherapeutic cytotoxic T lymphocytes. *Cell Metab.* **34**, 1342–1358.e1347 (2022).
- Lu, Z. et al. Tumor factors stimulate lysosomal degradation of tumor antigens and undermine their cross-presentation in lung cancer. *Nat. Commun.* **13**, 6623 (2022).
- Lund, A. W. et al. VEGF-C promotes immune tolerance in B16 melanomas and cross-presentation of tumor antigen by lymph node lymphatics. *Cell Rep.* **1**, 191–199 (2012).
- Ruiz, F. et al. Endothelial cell-derived oxysterol ablation attenuates experimental autoimmune encephalomyelitis. *EMBO Rep.* **24**, e55328 (2023).
- Naualaerts, S. et al. Multiomics and spatial mapping characterizes human CD8(+) T cell states in cancer. *Sci. Transl. Med.* **15**, eadd1016 (2023).
- Vanmeerbeek, I. et al. Early memory differentiation and cell death resistance in T cells predicts melanoma response to sequential anti-CTLA4 and anti-PD1 immunotherapy. *Genes Immun.* **22**, 108–119 (2021).
- Bazigou, E. et al. Genes regulating lymphangiogenesis control venous valve formation and maintenance in mice. *J. Clin. Investig.* **121**, 2984–2992 (2011).
- Arasa, J. et al. Upregulation of VCAM-1 in lymphatic collectors supports dendritic cell entry and rapid migration to lymph nodes in inflammation. *J. Exp. Med.* <https://doi.org/10.1084/jem.20201413> (2021).

25. Beck, K. R. et al. Enzymatic interconversion of the oxysterols 7beta,25-dihydroxycholesterol and 7-keto,25-hydroxycholesterol by 11beta-hydroxysteroid dehydrogenase type 1 and 2. *J. Steroid Biochem. Mol. Biol.* **190**, 19–28 (2019).
26. Liu, C. et al. Oxysterols direct B-cell migration through EB12. *Nature* **475**, 519–523 (2011).
27. Hannedouche, S. et al. Oxysterols direct immune cell migration via EB12. *Nature* **475**, 524–527 (2011).
28. Lu, E., Dang, E. V., McDonald, J. G. & Cyster, J. G. Distinct oxysterol requirements for positioning naive and activated dendritic cells in the spleen. *Sci. Immunol.* <https://doi.org/10.1126/sciimmunol.aal5237> (2017).
29. Sun, S. & Liu, C. 7alpha, 25-dihydroxycholesterol-mediated activation of EB12 in immune regulation and diseases. *Front. Pharm.* **6**, 60 (2015).
30. Kamensek, U. et al. Mutational burden, MHC-I expression and immune infiltration as limiting factors for in situ vaccination by TNFalpha and IL-12 gene electrotransfer. *Bioelectrochemistry* **140**, 107831 (2021).
31. Tewalt, E. F., Cohen, J. N., Rouhani, S. J. & Engelhard, V. H. Lymphatic endothelial cells - key players in regulation of tolerance and immunity. *Front. Immunol.* **3**, 305 (2012).
32. Pokharel, S. M. et al. Integrin activation by the lipid molecule 25-hydroxycholesterol induces a proinflammatory response. *Nat. Commun.* **10**, 1482 (2019).
33. Li, W. et al. Correlation between PD-1/PD-L1 expression and polarization in tumor-associated macrophages: A key player in tumor immunotherapy. *Cytokine Growth Factor Rev.* **67**, 49–57 (2022).
34. Tian, T. & Li, Z. Targeting Tim-3 in cancer with resistance to PD-1/PD-L1 blockade. *Front. Oncol.* **11**, 731175 (2021).
35. Liu, S. Y. et al. Interferon-inducible cholesterol-25-hydroxylase broadly inhibits viral entry by production of 25-hydroxycholesterol. *Immunity* **38**, 92–105 (2013).
36. Benner, B. et al. Generation of monocyte-derived tumor-associated macrophages using tumor-conditioned media provides a novel method to study tumor-associated macrophages in vitro. *J. Immunother. Cancer* **7**, 140 (2019).
37. Ries, C. H. et al. Targeting tumor-associated macrophages with anti-CSF-1R antibody reveals a strategy for cancer therapy. *Cancer Cell* **25**, 846–859 (2014).
38. Ghosh, A. et al. Increased p53 expression induced by APR-246 reprograms tumor-associated macrophages to augment immune checkpoint blockade. *J. Clin. Invest.* <https://doi.org/10.1172/JCI148141> (2022).
39. Trikha, P. et al. E2f3 in tumor macrophages promotes lung metastasis. *Oncogene* **35**, 3636–3646 (2016).
40. Bae, S. et al. MYC-mediated early glycolysis negatively regulates proinflammatory responses by controlling IRF4 in inflammatory macrophages. *Cell Rep.* **35**, 109264 (2021).
41. Collins, S. L. et al. mTORC1 signaling regulates proinflammatory macrophage function and metabolism. *J. Immunol.* **207**, 913–922 (2021).
42. Marelli, G. et al. Lipid-loaded macrophages as new therapeutic target in cancer. *J Immunother Cancer* <https://doi.org/10.1136/jitc-2022-004584> (2022).
43. Shi, H. et al. NLRP3 activation and mitosis are mutually exclusive events coordinated by NEK7, a new inflammasome component. *Nat. Immunol.* **17**, 250–258 (2016).
44. Deng, J. & Fleming, J. B. Inflammation and myeloid cells in cancer progression and metastasis. *Front. Cell Dev. Biol.* **9**, 759691 (2021).
45. Holland, S. J. et al. R428, a selective small molecule inhibitor of Axl kinase, blocks tumor spread and prolongs survival in models of metastatic breast cancer. *Cancer Res.* **70**, 1544–1554 (2010).
46. Lu, Q. et al. Tyro-3 family receptors are essential regulators of mammalian spermatogenesis. *Nature* **398**, 723–728 (1999).
47. Myers, K. V., Amend, S. R. & Pienta, K. J. Targeting Tyro3, Axl and MerTK (TAM receptors): implications for macrophages in the tumor microenvironment. *Mol. Cancer* **18**, 94 (2019).
48. Larionova, I., Kazakova, E., Patysheva, M. & Kzhyshkowska, J. Transcriptional, epigenetic and metabolic programming of tumor-associated macrophages. *Cancers* <https://doi.org/10.3390/cancers12061411> (2020).
49. Siddiqui, S. & Glauben, R. Fatty acid metabolism in myeloid-derived suppressor cells and tumor-associated macrophages: key factor in cancer immune evasion. *Cancers* <https://doi.org/10.3390/cancers14010250> (2022).
50. Pan, W. et al. The DNA methylcytosine dioxygenase Tet2 sustains immunosuppressive function of tumor-infiltrating myeloid cells to promote melanoma progression. *Immunity* **47**, 284–297 e285 (2017).
51. Cyster, J. G., Dang, E. V., Reboldi, A. & Yi, T. 25-Hydroxycholesterols in innate and adaptive immunity. *Nat. Rev. Immunol.* **14**, 731–743 (2014).
52. Toobian, D., Ghosh, P. & Katkar, G. D. Parsing the role of PPARs in macrophage processes. *Front. Immunol.* **12**, 783780 (2021).
53. Xu, L. et al. 25-Hydroxycholesterol-3-sulfate attenuates inflammatory response via PPARgamma signaling in human THP-1 macrophages. *Am. J. Physiol. Endocrinol. Metab.* **302**, E788–E799 (2012).
54. Plitas, G. et al. Regulatory T cells exhibit distinct features in human breast cancer. *Immunity* **45**, 1122–1134 (2016).
55. Raccosta, L. et al. The oxysterol-CXCR2 axis plays a key role in the recruitment of tumor-promoting neutrophils. *J. Exp. Med.* **210**, 1711–1728 (2013).
56. Bensinger, S. J. & Tontonoz, P. Integration of metabolism and inflammation by lipid-activated nuclear receptors. *Nature* **454**, 470–477 (2008).
57. Villablanca, E. J. et al. Tumor-mediated liver X receptor-alpha activation inhibits CC chemokine receptor-7 expression on dendritic cells and dampens antitumor responses. *Nat. Med.* **16**, 98–105 (2010).
58. Tavazoie, M. F. et al. LXR/ApoE activation restricts innate immune suppression in cancer. *Cell* **172**, 825–840.e818 (2018).
59. Xiao, J. et al. 25-Hydroxycholesterol regulates lysosome AMP kinase activation and metabolic reprogramming to educate immunosuppressive macrophages. *Immunity* **57**, 1087–1104.e1087 (2024).
60. Caronni, N. et al. IL-1beta(+) macrophages fuel pathogenic inflammation in pancreatic cancer. *Nature* **623**, 415–422 (2023).
61. Chittechath, M. et al. Molecular profiling reveals a tumor-promoting phenotype of monocytes and macrophages in human cancer progression. *Immunity* **41**, 815–829 (2014).
62. Kaplanov, I. et al. Blocking IL-1beta reverses the immunosuppression in mouse breast cancer and synergizes with anti-PD-1 for tumor abrogation. *Proc. Natl Acad. Sci. USA* **116**, 1361–1369 (2019).
63. Rebe, C. & Ghiringhelli, F. Interleukin-1beta and cancer. *Cancers* <https://doi.org/10.3390/cancers12071791> (2020).
64. Lee, P. H. et al. Host conditioning with IL-1beta improves the anti-tumor function of adoptively transferred T cells. *J. Exp. Med.* **216**, 2619–2634 (2019).
65. Tulotta, C. et al. IL-1B drives opposing responses in primary tumours and bone metastases; harnessing combination therapies to improve outcome in breast cancer. *NPJ Breast Cancer* **7**, 95 (2021).
66. Takahashi, H. et al. Cholesterol 25-hydroxylase is a metabolic switch to constrain T cell-mediated inflammation in the skin. *Sci. Immunol.* **6**, eabb6444 (2021).
67. Jiang, C., Ting, A. T. & Seed, B. PPAR-gamma agonists inhibit production of monocyte inflammatory cytokines. *Nature* **391**, 82–86 (1998).
68. Su, M. et al. The in vitro and in vivo anti-inflammatory effects of a phthalimide PPAR-gamma agonist. *Mar. Drugs* <https://doi.org/10.3390/md15010007> (2017).

69. Nelson, V. L. et al. PPARgamma is a nexus controlling alternative activation of macrophages via glutamine metabolism. *Genes Dev.* **32**, 1035–1044 (2018).
70. Antila, S. et al. Development and plasticity of meningeal lymphatic vessels. *J. Exp. Med.* **214**, 3645–3667 (2017).
71. Li, Z. et al. Blockade of VEGFR3 signaling leads to functional impairment of dural lymphatic vessels without affecting auto-immune neuroinflammation. *Sci. Immunol.* **8**, eabq0375 (2023).
72. Garnier, L. et al. IFN-gamma-dependent tumor-antigen cross-presentation by lymphatic endothelial cells promotes their killing by T cells and inhibits metastasis. *Sci. Adv.* **8**, eabl5162 (2022).
73. Broggi, M. A. S. et al. Tumor-associated factors are enriched in lymphatic exudate compared to plasma in metastatic melanoma patients. *J. Exp. Med.* **216**, 1091–1107 (2019).
74. Randolph, G. J., Angeli, V. & Swartz, M. A. Dendritic-cell trafficking to lymph nodes through lymphatic vessels. *Nat. Rev. Immunol.* **5**, 617–628 (2005).
75. Swartz, M. A. & Lund, A. W. OPINION lymphatic and interstitial flow in the tumour microenvironment: linking mechanobiology with immunity. *Nat. Rev. Cancer* **12**, 210–219 (2012).
76. El-Hajjaji, F. Z. et al. Liver X receptors, lipids and their reproductive secrets in the male. *Biochim. Biophys. Acta* **1812**, 974–981 (2011).
77. Schneider, C. et al. Induction of the nuclear receptor PPAR-gamma by the cytokine GM-CSF is critical for the differentiation of fetal monocytes into alveolar macrophages. *Nat. Immunol.* **15**, 1026–1037 (2014).
78. Neubert, N. J. et al. Broad and conserved immune regulation by genetically heterogeneous melanoma cells. *Cancer Res.* **77**, 1623–1636 (2017).
79. Voelter, V. et al. An unusual case of metastatic melanoma sensitive to chemotherapy and immunotherapy, with late immune escape in the brain. *Cancer Immun.* **8**, 6 (2008).
80. Hinshaw, D. C. & Shevde, L. A. The tumor microenvironment innately modulates cancer progression. *Cancer Res.* **79**, 4557–4566 (2019).
81. Preibisch, S., Saalfeld, S. & Tomancak, P. Globally optimal stitching of tiled 3D microscopic image acquisitions. *Bioinformatics* **25**, 1463–1465 (2009).
82. Dobin, A. et al. STAR: ultrafast universal RNA-seq aligner. *Bioinformatics* **29**, 15–21 (2013).
83. Quinlan, A. R. & Hall, I. M. BEDTools: a flexible suite of utilities for comparing genomic features. *Bioinformatics* **26**, 841–842 (2010).
84. Robinson, M. D., McCarthy, D. J. & Smyth, G. K. edgeR: a Bioconductor package for differential expression analysis of digital gene expression data. *Bioinformatics* **26**, 139–140 (2010).
85. Sprooten, J. et al. Lymph node and tumor-associated PD-L1(+) macrophages antagonize dendritic cell vaccines by suppressing CD8(+) T cells. *Cell Rep. Med.* **5**, 101377 (2024).
86. Kovacs, S. A. & Gyorffy, B. Transcriptomic datasets of cancer patients treated with immune-checkpoint inhibitors: a systematic review. *J. Transl. Med.* **20**, 249 (2022).
87. Lanczky, A. & Gyorffy, B. Web-based survival analysis tool tailored for medical research (KMplot): development and implementation. *J. Med. Internet Res.* **23**, e27633 (2021).
- our RNA sequencing data, and O. Vadas from the Protein Core Facility for antibody purification. Anti-CSFR1 antibodies producing hybridoma were generated by M. Merad and obtained from M. Ingersoll. EO771 cells were obtained from M. De Palma. Research in SH lab is supported by the Swiss Cancer League (KFS-5108-08-2020-R), the SNSF (310030_185255, 310030_215017), the Geneva Cancer League, and the Leenaards Foundation. Research in AD Garg lab is supported by Research Foundation Flanders (FWO) (Fundamental Research Grant, GOB4620N; FWO SBO grant for “ANTIBODY” consortium), KU Leuven (C3 grants, C3/21/037, and C3/22/022), VLIR-UOS (iBOF grant, iBOF/21/048, for “MIMICRY” consortium), and Olivia Hendrickx Research Fund (OHRF Immunobiomarkers).

Author contributions

Conceptualization and methodology: M.S., T.V.P., C.J., D.E.S., C.P., C.S., K.H., G.G.M., A.D.G., and S.H. Investigation: M.S., L.G., R.C., M.R., C.W., J.A., J.M., R.P., D.B., N.F., D.T., S.T., J-M.L., and M.K. Data validation and analysis: M.S., N.F., A.D.G., and S.H. Writing and editing: M.S., L.G., T.V.P., C.J., D.E.S., C.S., A.D.G., and S.H. Correspondence to Stéphanie Hugues.

Competing interests

The authors declare no competing interests.

Additional information

Supplementary information The online version contains supplementary material available at <https://doi.org/10.1038/s41467-025-55969-w>.

Correspondence and requests for materials should be addressed to Stéphanie Hugues.

Peer review information *Nature Communications* thanks the anonymous reviewer(s) for their contribution to the peer review of this work. A peer review file is available.

Reprints and permissions information is available at <http://www.nature.com/reprints>

Publisher's note Springer Nature remains neutral with regard to jurisdictional claims in published maps and institutional affiliations.

Open Access This article is licensed under a Creative Commons Attribution-NonCommercial-NoDerivatives 4.0 International License, which permits any non-commercial use, sharing, distribution and reproduction in any medium or format, as long as you give appropriate credit to the original author(s) and the source, provide a link to the Creative Commons licence, and indicate if you modified the licensed material. You do not have permission under this licence to share adapted material derived from this article or parts of it. The images or other third party material in this article are included in the article's Creative Commons licence, unless indicated otherwise in a credit line to the material. If material is not included in the article's Creative Commons licence and your intended use is not permitted by statutory regulation or exceeds the permitted use, you will need to obtain permission directly from the copyright holder. To view a copy of this licence, visit <http://creativecommons.org/licenses/by-nc-nd/4.0/>.

© The Author(s) 2025

Acknowledgements

We thank C. Gameiro, G. Schreiner, and L. Tran for excellent assistance in flow cytometry, D. Chollet and M. Docquier for excellent assistance in Q-PCR and sequencing experiments, S. Lemeille for analysing some of

¹Department of Pathology and Immunology; Geneva Medical School, Geneva, Switzerland. ²Metabolism and Nutrition Research Group, Walloon Excellence in Life sciences and BIOTEchnology (WELBIO), Louvain Drug Research Institute, Université catholique de Louvain, Brussels, Belgium. ³Translational Data Science (TDS), Swiss Institute of Bioinformatics (SIB), Lausanne, Switzerland. ⁴Swiss Cancer Center Leman, Lausanne, Switzerland. ⁵Department of Oncology, Center for Experimental Therapeutics, Lausanne University Hospital (CHUV), Lausanne, Switzerland. ⁶Ludwig Institute for Cancer Research, Lausanne, Switzerland. ⁷Université Clermont Auvergne, iGReD, CNRS UMR 6293, INSERM U1103, 28, place Henri Dunant, BP38, 63001 Clermont-Ferrand, France. ⁸Groupe Cancer Clermont Auvergne, 28, place Henri Dunant, BP38, 63001 Clermont-Ferrand, France. ⁹Centre de Recherche en Nutrition Humaine d’Auvergne, 58 Boulevard Montalembert, F-63009 Clermont-Ferrand, France. ¹⁰Department of Oncology, University of Lausanne, Lausanne, Switzerland. ¹¹Geneva Centre for Inflammation Research, Geneva, Switzerland. ¹²Translational Research Centre in Oncohaematology, Geneva, Switzerland. ¹³Institute of Molecular Health Sciences, Swiss Federal Institute of Technology (ETH), Zurich, Switzerland. ¹⁴Laboratories of Neuroimmunology, Service of Neurology and Neuroscience Research Center, Department of Clinical Neurosciences, Lausanne University Hospital and University of Lausanne, Lausanne, Switzerland. ¹⁵Biomedical Center (BMC), Institute for Cardiovascular Physiology and Pathophysiology, Walter-Brendel-Center for Experimental Medicine (WBex), Faculty of Medicine, Ludwig-Maximilians-Universität Munich, Planegg-Martinsried, Germany. ¹⁶Laboratory for Cell Stress & Immunity (CSI), Department of Cellular & Molecular Medicine (CMM), KU Leuven, Belgium. ¹⁷Present address: National Key Laboratory of Immunity and Inflammation, Suzhou Institute of Systems Medicine, Chinese Academy of Medical Sciences & Peking Union Medical College, Suzhou 215123 Jiangsu, China. ✉e-mail: stephanie.hugues@unige.ch